



Coherent and incoherent laser pump on a five-level atom in a strongly coupled cavity-QED systemAsha Devi ^{1,*}, Sarath D. Gunapala,² and Malin Premaratne ^{1,†}¹*Advanced Computing and Simulation Laboratory, Department of Electrical and Computer Systems Engineering, Monash University, Clayton, Victoria 3800, Australia*²*Jet Propulsion Laboratory, California Institute of Technology, Pasadena, California 91109, USA*

(Received 11 April 2021; revised 28 October 2021; accepted 13 December 2021; published 3 January 2022)

We propose a cavity quantum electrodynamic system consisting of a five-level atom coupled to a single mode of the cavity electromagnetic field. The study is focused on the regime of strong coupling between the cavity and atom. Pump laser fields and cavity fields connect the split energy levels of the atom. Instead of the well-known two-level Dicke model obtained by adiabatic elimination of the high-energy levels, we consider the pump lasers' detunings to the atomic transitions to be very small such that we can examine the influence of the higher-energy states. We have studied the effect of an external coherent drive and incoherent pumping on these higher-energy levels and observed the enhancement of intracavity photon numbers due to quantum coherence effects. The amplification of intracavity photons is achieved even without a population inversion. However, the effect of the coherent and incoherent drive is negligible for very large detunings when the higher-energy states are adiabatically eliminated. At zero and small detunings, the system reaches the steady state at an earlier instant of time for higher incoherent pumping. We find an almost agreeable steady-state behavior of the system's exact full quantum dynamics model and its semiclassical approximation. Our model tries to accurately simulate the open system by considering the cavity decay, spontaneous decay, and dephasing of the system.

DOI: [10.1103/PhysRevA.105.013701](https://doi.org/10.1103/PhysRevA.105.013701)**I. INTRODUCTION**

The interplay between the electromagnetic field and the atom leads to an exchange of energy between them and the theory of their interaction is explained in quantum electrodynamics (QED) [1–5]. Cavity QED addresses controlling of this interaction at a quantum level by placing an atom inside a resonator structure or cavity [6,7]. With the advancement in research, high- Q cavities are developed in which periodic exchange of photon between the atom and single-cavity mode takes place multiple times before any dissipative process occurs, which enhances the atom-cavity coupling strength [8]. A strong-coupling regime is reached when the coupling strength η exceeds the decay rates of the cavity and the atom [9,10]. Many systems are investigated to realize such a strong-coupling regime with the matter in the form of two-dimensional (2D) electron gas [11], artificial atoms such as quantum dot [12] or superconducting qubit [13], organic materials [14], inorganic quantum wells [15], and many more. Similarly, there exists a sizable body of work on different resonators to achieve such coupling regimes, namely high- Q factor Fabry-Perot resonator [16], monolithic microresonator [17], and toroidal shape silica microresonator [18].

The importance of a multilevel atom coupled with a pair of coherent lasers and cavity field is realized with the introduction of a four-level atom by Dimer *et al.* [19,20]. Considering such an atom, one can control the system parameters by

changing the pump laser frequency. As the counterrotating terms are taken into account the rotating-wave approximation is not applicable in this case. To facilitate the analysis, we map two low-lying states of the four-level atom to an effective two-level atom. We adiabatically eliminate the remaining two excited states of the four-level atom. Based on this system, a lot of work has been done to study the ground-state properties for over the years both experimentally and theoretically [21,22]. For example, exploring critical phase transition behavior for single atom by adding a nonlinear coupling term [23,24], adding additional dipole-dipole interaction terms to the existing system [25], experimental realization for better tunability of system parameters [26], and the list goes on.

However, none of these studies have explored the influence of the excited states on the system parameters. On the contrary, some recent theoretical studies on nanoplasmonics [27] demonstrate surface plasmon enhancement by applying coherent driving on the excited states. Therefore, in the present study, we intend to explore the excited states' effect in a strongly coupled atom-cavity system, which can provide a more complete and accurate picture of the system. We focus on a five-level atom pumped with both coherent and incoherent laser field. We present a model that can demonstrate a large enhancement of photon numbers by introducing the incoherent and coherent field to the fifth level. We observe a quantum coherence phenomenon that amplify photon numbers when we introduce the combination of incoherent and coherent drive to the excited states. The control over the fields may be important for obtaining ultrafast photonic applications [19,27]. We also have a faster approach to steady state for such a high magnitude of intracavity photons. This can be helpful

*asha.devi@monash.edu

†malin.premaratne@monash.edu

to avoid extensive heating, which would otherwise eventually decrease the lifetime of a device. Though the enhancement of photon numbers decreases with the introduction of dephasing, the system is still robust to high dephasing frequencies.

The detunings of the laser with the atomic transition frequencies are assumed to be small in comparison to the atom-cavity coupling, cavity decay, and spontaneous decay of the system. Provided this condition, we cannot adiabatically eliminate the excited states. We observe that in the steady-state regime, the intracavity photon numbers are enhanced due to the quantum coherence effect without undergoing population inversion. The system retains this significant characteristic even after introduction of dephasing. At small and zero detuning, the system reaches the steady state at a much earlier instant for large incoherent pumping. However, when the detunings are very large the effects of the additional coherent and incoherent drive are found to be negligible. The proposed model has been primarily studied for $N = 100$ atoms. Keeping in mind the importance of small number of atoms in quantum optics and quantum information processing [17], we also explore this case and the observations are found to be promising.

In this study, we consider the semiclassical approximations for solving the master equation of the proposed model. To verify the semiclassical model, we carry out a full quantum dynamics simulation of the system. Both models provide an almost agreeable steady-state solution for $N = 2$ atoms. However, the large Hilbert space requirement limits our quantum dynamics simulations to a small number of atoms.

The paper is structured as follows. The proposed model is formulated in Secs. II and III, providing the step by step formation of the Hamiltonian and the density matrix of open quantum system. In Sec. IV the system is analyzed numerically in the steady-state region to study the intracavity photon numbers for small and large detunings. The model is tested for small and large atoms, with and without dephasing. Section V shows the transient analysis of the system when the laser field is in resonance and off resonant with the atomic transition. The system is also analyzed for small and large values of incoherent pumping. In Sec. VI we provide a comparison of full quantum dynamics system with the semiclassical model. Section VII summarizes this work. The derivation of the Lindblad open quantum system is provided in Appendix A. The derivation of the reduced Hamiltonian obtained after adiabatic elimination of excited states is given in Appendix B. Appendix C gives the outline for the setup of our five-level system for quantum simulation required in PSIQUASP.

II. HAMILTONIAN FORMATION

We consider a system consisting of an ensemble of N atoms coupled to a single-mode of the cavity field. The multilevel atom presented in this paper is similar to the one studied in Refs. [19,26] and is illustrated in Fig. 1. We briefly introduce a possible cavity QED setup with the multilevel atom in the strong-coupling regime. The atoms are enclosed in a high-finesse optical cavity such as a silica microtoroid resonator with a principal cavity diameter of $50 \mu\text{m}$ and at a wavelength of $\sim 850 \text{ nm}$ [18]. Such a resonator provide ultrahigh- Q factor exceeding 10^8 , low cavity losses, and small mode volume V .

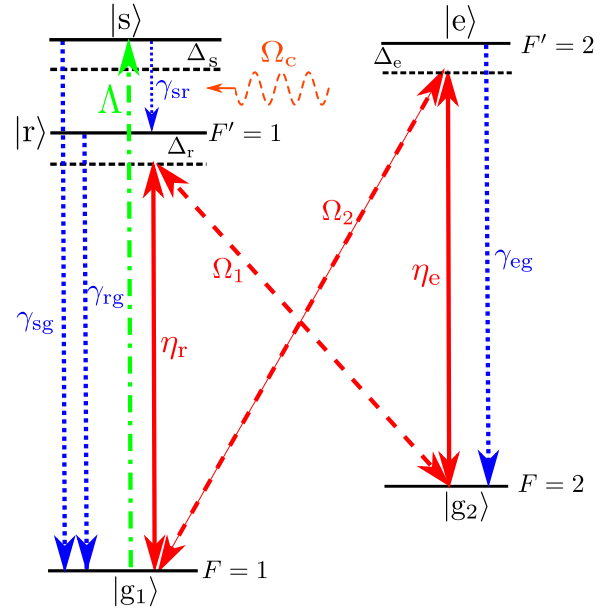


FIG. 1. Schematic of a multilevel atom with hyperfine ground levels $|g_1\rangle$ and $|g_2\rangle$, and excited states $|r\rangle$, $|s\rangle$ and $|e\rangle$ (not to scale). $|g_1\rangle$ is at zero energy and $|g_2\rangle$ is at an energy level of $\hbar\omega_g$. The solid lines (red) represent the atom-cavity coupling, the dashed lines (red) laser frequency terms, and dash-dot lines are the incoherent coupling (green). The curly dashed line is the external pump field applied (orange). The dotted lines represent the spontaneous decay rates from the excited states (blue).

The atoms and photons are assumed to be trapped close to the surface of the microtoroid and the atoms couple strongly to the evanescent fields of the whispering-gallery modes. Atoms approximately equal to $N = 100$ (a few dozen atoms) advance toward the evanescent field of resonator each time a small cloud of atoms are dropped at the proximity [17,28]. A strong-coupling rate of approximately $\eta/2\pi = 50 \text{ MHz}$ is achieved upon preliminary calculations at a certain distance of 45 nm from the microtoroid's surface [17]. Strong interactions of atom and field occurs if η exceeds the dissipation and decay parameters of the system, i.e., $\eta \gg \kappa, \gamma$. Here, γ represents the spontaneous dissipation of the atoms and κ is the cavity decay of the system to the environment.

The atoms inside the cavity are driven with two co-propagating lasers Ω_1 and Ω_2 . The laser beams are applied transverse to the cavity axis and are polarized linearly with the electric field of the cavity axis [26,29]. Both Ω_1 and Ω_2 are independently controllable beams. The atoms are considered to be identically coupled to the cavity mode [30]. We assume that interactions between the atoms are sufficiently weak so that the direct-dipole interactions can be neglected [31]. A magnetic field of $\approx 0.225 \text{ mT}$ is applied transverse to the laser fields to have a Zeeman splitting of the magnetic sublevels m of the atom [23,32]. The Stark and dispersive shifts between different m states are considered to be negligibly small [26].

The hyperfine structure of the multilevel atom depends on the values of orbital angular momentum L of the outer electron, spin angular momentum S , total electron angular momentum J , and nuclear angular momentum I [33]. The fine structure develops out of L and S resulting in $J = L + S$.

The hyperfine structure comes from coupling between J and I , and the total atomic angular momentum is given by $F = J + I$. Depending on different D line transition from ground to the excited states, we will have different values of F . The configuration in our paper employs the electric dipole transitions on the D_1 line of the atom, i.e., the transition from $|5^2S_{1/2}(F)\rangle \longleftrightarrow |5^2P_{1/2}(F')\rangle$, which is a part of fine-structure doublet [33]. Here, F and F' are the hyperfine levels in which the ground and excited states are present, respectively. The magnetic field splits the sublevels of the F ground state providing two ground states, one in the $F = 1$ level ($|g_1\rangle$) and one in the $F = 2$ level ($|g_2\rangle$). The excited states in the F' level are split into $F' = 1$ ($|r\rangle$) and $F' = 2$ level ($|s\rangle$ and $|e\rangle$) (Fig. 1). The $|g_1\rangle$ and $|g_2\rangle$ states are separated by a frequency of $\omega_g = 2\pi \times 6.835$ GHz and the hyperfine splitting frequency between $F' = 1$ and $F' = 2$ is $2\pi \times 812$ MHz [23,29,33]. The ground states $|g_1\rangle$ and $|g_2\rangle$ are coupled with the two pairs of laser fields (Ω_1, Ω_2) and the cavity fields [19,33]. The energy levels $\{|g_1\rangle, |e\rangle\}$ are connected by laser Rabi frequency Ω_2 and $\{|g_2\rangle, |r\rangle\}$ by Ω_1 . The transition from $|g_1\rangle$ to $|r\rangle$ and $|g_2\rangle$ to $|e\rangle$ is mediated by the cavity field strength η_r and η_e , respectively. When the atom goes from $|g_1\rangle$ to $|g_2\rangle$, i.e., raising to a higher-energy level, it provides a photon to the cavity. While following the inverse route to the lower state, it absorbs a photon from the cavity [20]. The atom is subjected to an additional coherent field Ω_c to couple the excited states $|r\rangle$ and $|s\rangle$ [27]. The transition between $|r\rangle$ to $|s\rangle$ is not coupled to the cavity mode as the frequency domain of the transitions $|g_1\rangle$ to $|r\rangle$ and $|r\rangle$ to $|s\rangle$ are different [27]. An incoherent pumping (Λ) populates the state $|s\rangle$ from the ground state $|g_1\rangle$ as direct transition between the states is not possible [34,35]. Under more realistic conditions the spontaneous decays of the excited states must be taken into account [32]. The state $|s\rangle$ decays to the state $|r\rangle$ at rate γ_{sr} and the relaxation rates γ_{rg} and γ_{eg} are from the states $|r\rangle \rightarrow |g_1\rangle$ and $|e\rangle \rightarrow |g_2\rangle$, respectively. In addition to that, a relaxation from the state $|s\rangle$ to the state $|g_1\rangle$ at rate γ_{sg} is also possible.

Our model is based on the semiclassical laser theory where the laser fields are treated classically and cavity field is treated quantum mechanically. The Hamiltonian \hat{H} is built using four parts, which are,

$$\hat{H} = \hat{H}_C + \hat{H}_A + \hat{H}_{CA} + \hat{H}_{LA}. \quad (1)$$

The term \hat{H}_C stands for the cavity Hamiltonian, \hat{H}_A for atomic terms, \hat{H}_{CA} for cavity-atom, and \hat{H}_{LA} for atom-laser coupling Hamiltonian. Expanding each of these terms in bra-ket notation [25]:

$$\hat{H}_C = \hbar\omega_c \hat{a}^\dagger \hat{a}, \quad (2a)$$

$$\hat{H}_A = \sum_{j=1}^N [\hbar(\omega_g |g_{2j}\rangle \langle g_{2j}| + \omega_e |e_j\rangle \langle e_j| + \omega_r |r_j\rangle \langle r_j| + \omega_s |s_j\rangle \langle s_j|)], \quad (2b)$$

with $|g_{1j}\rangle$ being at zero energy,

$$\hat{H}_{CA} = \sum_{j=1}^N [\hbar(\hat{a}^\dagger |g_{1j}\rangle \langle r_j| \eta_r + \hat{a}^\dagger |g_{2j}\rangle \langle e_j| \eta_e) + \text{H.c.}], \quad (2c)$$

$$\hat{H}_{LA} = \sum_{j=1}^N [\hbar(\Omega_1 e^{-i\omega_r t} |r_j\rangle \langle g_{2j}| e^{ikx} + \Omega_2 e^{-i\omega_e t} \times |e_j\rangle \langle g_{1j}| e^{ikx} + \Omega_c e^{-i\omega_s t} |s_j\rangle \langle r_j| e^{ikx}) + \text{H.c.}], \quad (2d)$$

We consider all the fields to be co-propagating along the tangential direction of the toroid with wave number k , and x is the position of the atom. The radiation wavelength is considered to be large enough so that the whole atom ensemble is concentrated together and coupled identically to the single mode of the field [36]. We assume that all atoms are positioned such that x can be set to a constant value for all of them, i.e., the atoms are considered to be trapped and atomic motions are negligible. In a realistic scenario, this assumption is considerably hard to satisfy [37]. Here, \hbar is the Planck's constant, H.c. denotes Hermitian conjugate. \hat{a} and \hat{a}^\dagger are the annihilation and creation operator of the cavity field, respectively. ω_c is the cavity frequency; ω_g , ω_r , ω_s , and ω_e are the atomic frequencies of the different energy levels as shown in Fig. 1. The frequencies of the driving lasers are ω_{lr} , ω_{le} and ω_{ls} . Atom-cavity coupling strength are represented as η_r and η_e between $|g_1\rangle \leftrightarrow |r\rangle$ and $|g_2\rangle \leftrightarrow |e\rangle$. In absence of the driving laser Ω_c , Eq. (1) simplifies to the Hamiltonian derived in Ref. [19].

The above Hamiltonian [Eq. (1)] is in the Schrödinger picture and we are interested in the interaction picture. We transform the system Hamiltonian to a rotating frame introducing the unitary transformation $\hat{U}(t) = \exp(-\frac{i}{\hbar} \hat{H}_0 t)$ [20], with

$$\begin{aligned} \hat{H}_0 = \sum_{j=1}^N & \left[\frac{1}{2}(\omega_{lr} + \omega_{le}) \hat{a}^\dagger \hat{a} + \frac{1}{2}(\omega_{le} - \omega_{lr}) |g_{2j}\rangle \langle g_{2j}| \right. \\ & + \omega_{le} |e_j\rangle \langle e_j| + \left. \left\{ \omega_{ls} + \frac{1}{2}(\omega_{lr} + \omega_{le}) \right\} |s_j\rangle \langle s_j| \right. \\ & \left. + \frac{1}{2}(\omega_{lr} + \omega_{le}) |r_j\rangle \langle r_j| \right]. \quad (3) \end{aligned}$$

We consider that the frequency difference between ω_{le} and ω_{lr} of the laser fields Ω_2 and Ω_1 is approximately equal to twice the hyperfine splitting of the ground-state frequency ω_g i.e., $\omega_{le} - \omega_{lr} \approx 2\omega_g$ [20,23]. Considering this the Hamiltonian in the interaction picture after the evolution is given by,

$$\begin{aligned} \hat{H}_{in} = \hbar\Delta_{cav} \hat{a}^\dagger \hat{a} + \sum_{j=1}^N & [\hbar\Delta_s |s_j\rangle \langle s_j| + \hbar\Delta_e |e_j\rangle \langle e_j| \\ & + \hbar\Delta_r |r_j\rangle \langle r_j| + \hbar\Delta_g |g_{2j}\rangle \langle g_{2j}| + \hat{H}_{LA}(0) + \hat{H}_{CA}], \quad (4) \end{aligned}$$

and the detunings in the above equation are defined as,

$$\Delta_e = \omega_e - \omega_{le}, \quad (5a)$$

$$\Delta_s = \omega_s - \omega_{ls}, \quad (5b)$$

$$\Delta_{cav} = \omega_c - \frac{\omega_{lr} + \omega_{le}}{2}, \quad (5c)$$

$$\Delta_r = \omega_r - \frac{\omega_{lr} + \omega_{le}}{2}, \quad (5d)$$

$$\Delta_g = \omega_g - \frac{\omega_{le} - \omega_{lr}}{2}. \quad (5e)$$

III. OPEN QUANTUM SYSTEM

The previous section gives us details on setting up the system Hamiltonian. In order to understand how the system evolves with time t , in this section we study the time evolution of the density matrix $\hat{\rho}_s(t)$, which describes the state of the system [2,38]. Because we have an open quantum system, the dynamics of this density matrix is described by the quantum Lindblad master equation [39–41]. The versatility of this formulation is that it can incorporate the spontaneous emission and cavity decay of the system to the environment [42]. The Lindblad master equation for the proposed system can be written as [7],

$$\dot{\hat{\rho}}_s = -\frac{i}{\hbar}[\hat{H}_{\text{in}}, \hat{\rho}_s] + \mathcal{L}_c[\hat{\rho}_s] + \frac{\gamma_{\downarrow}}{2}\mathcal{L}_{J_-}[\hat{\rho}_s] + \frac{\gamma_{\uparrow}}{2}\mathcal{L}_{J_+}[\hat{\rho}_s], \quad (6)$$

where $\mathcal{L}_c[\hat{\rho}_s]$, $\mathcal{L}_{J_-}[\hat{\rho}_s]$, and $\mathcal{L}_{J_+}[\hat{\rho}_s]$ are the Lindblad superoperators denoting cavity decay, spontaneous emission, and incoherent pumping such that $\mathcal{L}_{\hat{O}}[\hat{\rho}_s] = (2\hat{O}\hat{\rho}_s\hat{O}^\dagger - \hat{O}^\dagger\hat{O}\hat{\rho}_s - \hat{\rho}_s\hat{O}^\dagger\hat{O})$ with $\hat{O} = \{c, J_-, J_+\}$. The population decay rate coefficient is γ_{\downarrow} , which represents emissions, γ_{\uparrow} is the coefficient of population gain, and κ is the cavity decay rate of the system to the environment [36]. The derivation of Lindblad master equation is summarized in Appendix A.

As the atoms are confined to a small region smaller than the wavelength of light, the atoms will emit light superradiantly. The spontaneous emission therefore will be represented by collective spin operators given by: $\hat{J}_- = \sum_n \hat{\sigma}_{-,n}$ and $\hat{J}_+ = \sum_n \hat{\sigma}_{+,n}$ [36]. Summarizing the Lindblad superoperator terms as described in Appendix A, we have,

$$\begin{aligned} \mathcal{L}_c[\hat{\rho}_s] &= \kappa(2\hat{a}\hat{\rho}_s\hat{a}^\dagger - \hat{a}^\dagger\hat{a}\hat{\rho}_s - \hat{\rho}_s\hat{a}^\dagger\hat{a}), \\ \frac{\gamma_{\downarrow}}{2}\mathcal{L}_{J_-}[\hat{\rho}_s] &= \sum_{j=1}^N \left[\frac{\gamma_{\text{sr}}}{2}(2\hat{J}_{\text{rs}}^j\hat{\rho}_s\hat{J}_{\text{sr}}^j - \hat{J}_{\text{sr}}^j\hat{J}_{\text{rs}}^j\hat{\rho}_s - \hat{\rho}_s\hat{J}_{\text{sr}}^j\hat{J}_{\text{rs}}^j) \right. \\ &\quad + \frac{\gamma_{\text{rg}}}{2}(2\hat{J}_{\text{gr}}^j\hat{\rho}_s\hat{J}_{\text{rg}}^j - \hat{J}_{\text{rg}}^j\hat{J}_{\text{gr}}^j\hat{\rho}_s - \hat{\rho}_s\hat{J}_{\text{rg}}^j\hat{J}_{\text{gr}}^j) \\ &\quad + \frac{\gamma_{\text{eg}}}{2}(2\hat{J}_{\text{ge}}^j\hat{\rho}_s\hat{J}_{\text{eg}}^j - \hat{J}_{\text{eg}}^j\hat{J}_{\text{ge}}^j\hat{\rho}_s - \hat{\rho}_s\hat{J}_{\text{eg}}^j\hat{J}_{\text{ge}}^j) \\ &\quad \left. + \frac{\gamma_{\text{sg}}}{2}(2\hat{J}_{\text{gs}}^j\hat{\rho}_s\hat{J}_{\text{sg}}^j - \hat{J}_{\text{sg}}^j\hat{J}_{\text{gs}}^j\hat{\rho}_s - \hat{\rho}_s\hat{J}_{\text{sg}}^j\hat{J}_{\text{gs}}^j) \right], \\ \frac{\gamma_{\uparrow}}{2}\mathcal{L}_{J_+}[\hat{\rho}_s] &= \sum_{j=1}^N \frac{\Lambda}{2}(2\hat{J}_{\text{gs}}^j\hat{\rho}_s\hat{J}_{\text{gs}}^j - \hat{J}_{\text{gs}}^j\hat{J}_{\text{gs}}^j\hat{\rho}_s - \hat{\rho}_s\hat{J}_{\text{gs}}^j\hat{J}_{\text{gs}}^j). \quad (7) \end{aligned}$$

Now, after discussing the formation of the system Hamiltonian and Lindblad master equation, we move forward to understand the dynamics involved in our model. In order to interpret that, we study the semiclassical dynamics of our open cavity system containing both large and small number of atoms. This study helps us to gauge the general behavior of the system and understand time-dependent open-cavity experiments performed [22,43]. As mentioned earlier, our model is built on the multilevel system proposed by Dimer *et al.*, which by its assumptions valid for a large number of atoms in the strong-coupling regime [19]. In such a coupling regime, the atom-cavity coupling parameter η is larger than the dissipation rates γ , and the decay rates of the system κ . In that particular study, along with the various theoretical and experimental studies (nonequilibrium Bose-Einstein condensate) based on

it, they have considered the semiclassical approximation of the steady states in the strong-coupling scenario for large number of atoms [21,26,43]. The semiclassical approximation is a good indicator of the general behavior of a system. The factorization of the mean values of operators are performed in this approximation and the quantum fluctuations effects are neglected. For, e.g., the factorization of mean values of operators $\langle \hat{a}\hat{\sigma}_i \rangle$ is represented as $\langle \hat{a}\hat{\sigma}_i \rangle = \langle \hat{a} \rangle \langle \hat{\sigma}_i \rangle$ and $\langle \hat{a}^\dagger\hat{\sigma}_i \rangle$ is given by $\langle \hat{a}^\dagger \rangle \langle \hat{\sigma}_i \rangle$ [20]. We have introduced the c -number variable $\langle \hat{a} \rangle = \alpha$ where α is the complex field representing classical quantities.

The elements of the density matrix $\hat{\rho}_s$ are basically the expectation values of the collective operators involved. As we can see that in Eq. (4) and Eq. (7) there is a summation over N term, we define collective spin operators to find the equation of motion [44,45]. To be more explicit we define $\hat{J}_{\text{sr}} = \sum_{j=1}^N |s_j\rangle\langle r_j|$ and $\hat{J}_{\text{rs}} = \sum_{j=1}^N |r_j\rangle\langle s_j|$ as done in the Dicke model [19]. Therefore, the elements of the density matrix for, e.g., $\rho_{\text{sr}} = \langle \hat{J}_{\text{sr}} \rangle$. It goes similarly for the other transitions. We can therefore determine the following complex valued coupled partial differential equations given by Eq. (8) from Eq. (6). This is achieved by using the definition that $\langle \hat{O} \rangle = \text{tr}[\hat{\rho}\hat{O}]$ and then finding the equation of motion for the operator $\langle \hat{O} \rangle$ [25,46,47],

$$\begin{aligned} \dot{\rho}_{\text{rg}_1} &= i\Delta_r\rho_{\text{rg}_1} + i\Omega_c\rho_{\text{s}_{\text{g}_1}} + i\Omega_1\rho_{\text{g}_2\text{g}_1} - i\Omega_2\rho_{\text{re}} \\ &\quad - i\eta_r\alpha^*(\rho_{\text{rr}} - \rho_{\text{g}_1\text{g}_1}) - \gamma_{\text{ph}}\rho_{\text{rg}_1} - \frac{1}{2}(\gamma_{\text{rg}_1} + \Lambda)\rho_{\text{rg}_1}, \quad (8a) \end{aligned}$$

$$\begin{aligned} \dot{\rho}_{\text{sr}} &= -i\Delta_r\rho_{\text{sr}} + \left[i\Delta_s - \frac{1}{2}(\gamma_{\text{sr}} + \gamma_{\text{rg}} + \gamma_{\text{sg}}) \right] \rho_{\text{sr}} - \gamma_{\text{ph}}\rho_{\text{sr}} \\ &\quad - i\Omega_1\rho_{\text{s}_{\text{g}_2}} - i\Omega_c(\rho_{\text{ss}} - \rho_{\text{rr}}) - i\eta_r\alpha\rho_{\text{s}_{\text{g}_1}}, \quad (8b) \end{aligned}$$

$$\begin{aligned} \dot{\rho}_{\text{eg}_2} &= -i\eta_e\alpha^*\{\rho_{\text{ee}} - \rho_{\text{g}_2\text{g}_2}\} + \left[i\Delta_e - i\Delta_g - \frac{\gamma_{\text{eg}_2}}{2} - \gamma_{\text{ph}} \right] \\ &\quad \times \rho_{\text{eg}_2} - i\Omega_1\rho_{\text{re}}^* + i\Omega_2\rho_{\text{g}_2\text{g}_1}^*, \quad (8c) \end{aligned}$$

$$\begin{aligned} \dot{\rho}_{\text{g}_2\text{g}_1} &= i\Omega_1\rho_{\text{rg}_1} - i\Omega_2\rho_{\text{eg}_2}^* - i\alpha^*\eta_r\rho_{\text{rg}_2}^* + i\alpha\eta_e\rho_{\text{eg}_1} \\ &\quad - \frac{1}{2}(\Lambda + 2\gamma_{\text{ph}})\rho_{\text{g}_2\text{g}_1}, \quad (8d) \end{aligned}$$

$$\begin{aligned} \dot{\rho}_{\text{se}} &= -i\Omega_2\rho_{\text{s}_{\text{g}_1}} + i\Omega_c\rho_{\text{re}} - i\alpha\eta_e\rho_{\text{s}_{\text{g}_2}} \\ &\quad - \frac{1}{2}\{(\gamma_{\text{sr}} + \gamma_{\text{eg}} + \gamma_{\text{sg}}) + 2i\Delta_e + 2\gamma_{\text{ph}}\}\rho_{\text{se}}, \quad (8e) \end{aligned}$$

$$\begin{aligned} \dot{\rho}_{\text{re}} &= i\Delta_r\rho_{\text{re}} + i\Omega_1\rho_{\text{g}_2\text{e}} - i\Omega_2\rho_{\text{rg}_1} + i\Omega_c\rho_{\text{se}} + i\alpha^*\eta_r\rho_{\text{g}_1\text{e}} \\ &\quad - i\alpha\eta_e\rho_{\text{rg}_2} - \frac{1}{2}\{(\gamma_{\text{rg}} + \gamma_{\text{eg}}) + 2i\Delta_e + 2\gamma_{\text{ph}}\}\rho_{\text{re}}, \quad (8f) \end{aligned}$$

$$\begin{aligned} \dot{\rho}_{\text{rg}_2} &= -i\Omega_1(\rho_{\text{rr}} - \rho_{\text{g}_2\text{g}_2}) + i\Omega_c\rho_{\text{s}_{\text{g}_2}} + i\alpha^*\eta_r\rho_{\text{g}_1\text{g}_2} \\ &\quad - i\alpha^*\eta_e\rho_{\text{re}} - \frac{1}{2}(\gamma_{\text{rg}} + 2\gamma_{\text{ph}})\rho_{\text{rg}_2} + i\Delta_r\rho_{\text{rg}_2}, \quad (8g) \end{aligned}$$

$$\begin{aligned} \dot{\rho}_{\text{eg}_1} &= -i\Omega_2(\rho_{\text{ee}} - \rho_{\text{g}_1\text{g}_1}) - i\alpha^*\eta_r\rho_{\text{er}} + i\alpha^*\eta_e\rho_{\text{g}_2\text{g}_1} \\ &\quad + \left[i\Delta_e - \frac{1}{2}\{\gamma_{\text{eg}} + \Lambda\} - \gamma_{\text{ph}} \right] \rho_{\text{eg}_1}, \quad (8h) \end{aligned}$$

$$\dot{\rho}_{\text{sg}_1} = \left[i\Delta_s - \frac{1}{2}\{(\gamma_{\text{sr}} + \gamma_{\text{sg}}) + \Lambda + 2\gamma_{\text{ph}}\} \right] \rho_{\text{sg}_1} - i\Omega_2 \rho_{\text{se}} + i\Omega_c \rho_{\text{rg}_1} - i\eta_r \alpha^* \rho_{\text{sr}}, \quad (8i)$$

$$\dot{\rho}_{\text{sg}_2} = -i\Omega_1 \rho_{\text{sr}} + i\Omega_c \rho_{\text{rg}_2} - i\alpha^* \eta_e \rho_{\text{se}} - \frac{1}{2}\{(\gamma_{\text{sr}} + \gamma_{\text{sg}}) + 2\gamma_{\text{ph}}\} \rho_{\text{sg}_2}, \quad (8j)$$

$$\dot{\rho}_{\text{g}_1\text{g}_1} = i[\Omega_2 \rho_{\text{eg}_1} - \Omega_2 \rho_{\text{g}_1\text{e}}] + i\eta_r [\alpha \rho_{\text{rg}_1} - \alpha^* \rho_{\text{g}_1\text{r}}] + \gamma_{\text{rg}} \rho_{\text{rr}} + \gamma_{\text{sg}} \rho_{\text{ss}} - \Lambda \rho_{\text{g}_1\text{g}_1}, \quad (8k)$$

$$\dot{\rho}_{\text{g}_2\text{g}_2} = i[\Omega_1 \rho_{\text{rg}_2} - \Omega_1 \rho_{\text{g}_2\text{r}}] + \gamma_{\text{eg}} \rho_{\text{ee}} + i\eta_e [\alpha \rho_{\text{eg}_2} - \alpha^* \rho_{\text{g}_2\text{e}}], \quad (8l)$$

$$\dot{\rho}_{\text{ss}} = i[\Omega_c \rho_{\text{rs}} - \Omega_c \rho_{\text{sr}}] + \Lambda \rho_{\text{g}_1\text{g}_1} - (\gamma_{\text{sr}} + \gamma_{\text{sg}}) \rho_{\text{ss}}, \quad (8m)$$

$$\dot{\rho}_{\text{ee}} = i[\Omega_2 \rho_{\text{eg}_1}^* - \Omega_2 \rho_{\text{eg}_1}] - \gamma_{\text{eg}} \rho_{\text{ee}} + i\eta_e [\alpha^* \rho_{\text{eg}_2}^* - \alpha \rho_{\text{eg}_2}], \quad (8n)$$

$$\rho_{\text{g}_1\text{g}_1} + \rho_{\text{g}_2\text{g}_2} + \rho_{\text{ss}} + \rho_{\text{ee}} + \rho_{\text{rr}} = 1, \quad (8o)$$

$$\dot{\alpha} = -(i\Delta_{\text{cav}} + \kappa)\alpha - iN[\eta_r \rho_{\text{g}_1\text{r}} + \eta_e \rho_{\text{g}_2\text{e}}]. \quad (8p)$$

The diagonal components $\{\rho_{\text{g}_1\text{g}_1}, \rho_{\text{g}_2\text{g}_2}\}$ represent the populations of the ground states, and $\{\rho_{\text{ee}}, \rho_{\text{rr}}, \rho_{\text{ss}}\}$ the populations of the excited states, respectively. By conservation of population, which can only be transferred between the above-mentioned states we have, $\rho_{\text{g}_1\text{g}_1} + \rho_{\text{g}_2\text{g}_2} + \rho_{\text{ss}} + \rho_{\text{ee}} + \rho_{\text{rr}} = 1$ [27]. We also assume that the nondiagonal elements of the density matrix has a phase relaxation (or dephasing) rate of γ_{ph} .

In order to solve Eq. (8) the nondiagonal density matrix elements are written in the form $\rho_{\text{cd}} = \text{Re}(\rho_{\text{cd}}) + i\text{Im}(\rho_{\text{cd}})$ and complex variable $\alpha = \text{Re}(\alpha) + i\text{Im}(\alpha)$. A total of 27 nonlinear, coupled differential equations are formed by equating the real and imaginary parts of the equation. All other variables are assumed to be real.

IV. STEADY-STATE ANALYSIS

The main purpose of the study is to see how the system observables behave in the presence of driven laser field Ω_c and incoherent pumping Λ . To simplify our system we follow the experimental realizations, which couple Bose-Einstein condensate to optical cavity [22], and cavity-assisted Raman transition in an open quantum system [21,26,29]. In these studies the atom-cavity coupling strength is taken intrinsically the same and therefore in our case we take $\eta_e = \eta_r = \eta$. We consider both the resonant and off-resonant nature of the laser fields with the atomic transitions. However, it is necessary that the relation,

$$\Delta_e, \Delta_r, \Delta_s \ll \kappa, \gamma, \eta_{r,e}, \Omega_{1,2,c}, \quad (9)$$

is true. When the laser fields are near resonance with the frequencies of atomic transition, the dynamics of the transition from $|g_1\rangle \rightarrow |e\rangle$ and $|g_2\rangle \rightarrow |r\rangle$ occur nearly with the same time scale as $|g_1\rangle \rightarrow |g_2\rangle$ and $|g_2\rangle \rightarrow |g_1\rangle$. In such a case the excited states $|e\rangle$ and $|r\rangle$ cannot be adiabatically eliminated [20]. The cavity field is considered to be in resonance with the laser pump frequencies, i.e., $\Delta_{\text{cav}} = 0$ [17,34]. In Sec. IV A we analyze the case with small detunings. This assumption is defensible as there is always endeavor to achieve near or perfectly resonant coupling [27,34].

In order to observe the full dynamics of the system [Eq. (6)], it is necessary that the atom-cavity coupling is stronger than the dissipation mechanisms [18,23]. As discussed in Sec. II we consider a cavity QED setup with a toroidal microresonator. The values and physical parameters of Ω_1 , Ω_2 , η , κ , and γ are taken from the experimental studies and the theoretical models [17,18,23,24]. Specifically, the values of the parameters are; spontaneous decay rates as $\gamma/2\pi = 2.6$ MHz, cavity decay rate as $\kappa/2\pi = 0.02$ MHz, and cavity-atom coupling strength $\eta/2\pi = 50$ MHz, laser beams $\{\Omega_1/2\pi = -470$, and $\Omega_2/2\pi = -780\}$ MHz. Also, as $\kappa < \eta$, this system is considered as a good-cavity system [44,45]. It is noted that all the values are taken in the acceptable numeric range when working in the strong-coupling regime as there is high degree of flexibility in the values that these parameters can take [31]. However, we do not compare our study with the previous studies done as our sole purpose is to study the effect of the coherent laser field Ω_c and incoherent laser field Λ . The value of Ω_c is taken nearly equal to the transition frequencies between the excited states $F' = 1$ and $F' = 2$, i.e., $-2\pi \times 800$ MHz as mentioned in Refs. [23,33] and many other papers. The value of Λ is varied in the GHz range owing to the transition between $F = 1$ and $F' = 2$ level.

To study the intracavity photon numbers $|\alpha|^2$, three different cases of Ω_c are considered: $\Omega_c = 0$, $\Omega_c < \Omega_1, \Omega_2$, and $\Omega_c > \Omega_2$. Primarily, we have considered the number of atoms $N = 100$. We will also see later how the system performs for very small number of atoms.

A. Intracavity photon numbers

We choose a small value for the detunings where adiabatic elimination of the excited states are not possible. Particularly, we take $\Delta_s = \Delta_g = \Delta_e = \Delta_r = -0.01 \times 2\pi$ MHz, which is less than the cavity decay rate $\kappa = 0.02 \times 2\pi$ MHz and spontaneous emission rate $\gamma = 2.6 \times 2\pi$ MHz for the above condition is satisfied. Small values of $\Omega_c/2\pi = \{0, -50\}$ MHz has a negligible effect on the photon numbers $|\alpha|^2$ [Fig. 2(a)] while they have a pronounced effect for $\Omega_c/2\pi = \{-800, -900\}$ MHz [Fig. 2(b)]. $|\alpha|^2$ enhances manifold with the increase in coherent coupling Ω_c and incoherent coupling Λ [Fig. 2(b)]. The amplification of the photon numbers is due to the quantum coherence phenomenon. When a strong coherent field is applied to the higher excited states, it leads to the quantum coherence phenomenon where the atoms are coupled. However, when Ω_c is very small say $\Omega_c/2\pi = -50$ MHz, the coherence phenomenon disappears. The steplike behavior of the intracavity photon numbers when $\Omega_c/2\pi = \{0, -50\}$ MHz is due the absence of quantum coherence near $\Lambda \approx 0.08$ GHz. In the absence of the coherence phenomenon, the atoms act independently and are unrelated to each other [48]. In such a situation, the collective photon average goes to zero or a very small value. Another additional observation is that the lasing threshold for $\Omega_c/2\pi = \{-800, -900\}$ MHz is reduced and achieved around $\Lambda \approx 0.06$ GHz.

The population inversion between the states $|g_1\rangle$ and $|r\rangle$ for the same detuning values are shown in Fig. 2(c) for $\Omega_c/2\pi = \{0, -50\}$ MHz and in Fig. 2(d) for $\Omega_c/2\pi = \{-500, -800, -900\}$ MHz. We observe an increase in

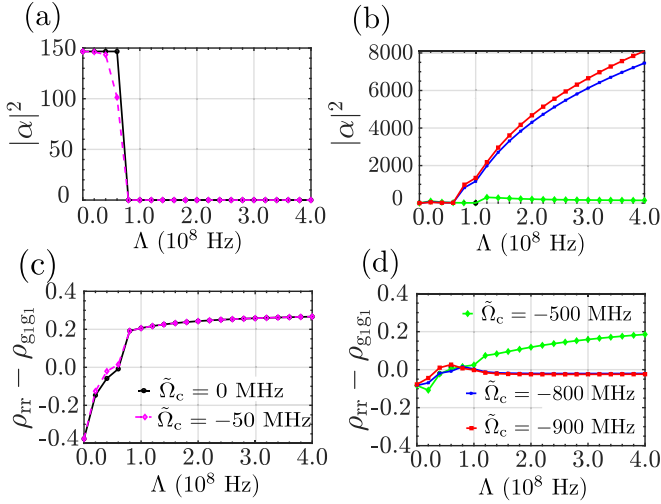


FIG. 2. Intracavity photon number $|\alpha|^2$ variation with incoherent pumping Λ for different values of coherent pumping $\tilde{\Omega}_c = \Omega_c/2\pi$ and $\eta/2\pi = 50$ MHz. In this case, the detunings of laser pumping with atomic transitions are considered as $\Delta_s = \Delta_g = \Delta_e = \Delta_r = -0.01 * 2\pi$ MHz. In (a) we show the $|\alpha|^2$ variation with Λ for very small values of $\Omega_c/2\pi = \{0, -50\}$ MHz. In (b) we do the same variation but for large values of $\Omega_c/2\pi = \{-500, -800, -900\}$ MHz. As can be seen Ω_c controls the generation of $|\alpha|^2$, which increases manifold for very large values of Ω_c . The population inversion between the states $|g_1\rangle$ and $|r\rangle$ is studied for $\Omega_c/2\pi = \{0, -50\}$ MHz in (c) and $\Omega_c/2\pi = \{-500, -800, -900\}$ MHz in (d). Quantum coherence by the coherent drive Ω_c leads to amplification of number of intracavity photons with no population inversion for $\Omega_c/2\pi = \{-800, -900\}$ MHz. The other parameter values are taken as $\Omega_1/2\pi = -470$ MHz, $\Omega_2/2\pi = -780$ MHz, the dephasing rate is $\gamma_{ph} = 0$, cavity decay $\kappa/2\pi = 0.02$ MHz and spontaneous decay $\gamma/2\pi = 2.6$ MHz.

population inversion in Fig. 2(c) as Λ increases for small values of Ω_c though accompanied by a decrease in $|\alpha|^2$. The reason $|\alpha|^2$ does not increase with increase in the population inversion is the absence of the quantum coherence phenomenon. However, even for no population inversion with an increase in Λ value for $\Omega_c/2\pi = \{-800, -900\}$ MHz [Fig. 2(d)], the photon number increases. Therefore, an enhancement in $|\alpha|^2$ is achieved due to the quantum coherence phenomenon even without a population inversion by controlling Ω_c .

B. Large detuning: Adiabatic elimination

We also intend to study the case when the detunings have a very large value, i.e., the condition:

$$\Delta_r, \Delta_s, \Delta_e \gg \kappa, \gamma, \eta_{r,e}, \Omega_{1,2,c}, \quad (10)$$

holds true. We choose such detuning value from Ref. [23], where the adiabatic elimination is satisfied. In line with such previous studies we understand that the influence of Ω_c and Λ should be minimum on the system as the excited states are to be adiabatically eliminated for such a high detuning value [19]. The elimination is justified only for very large detunings of the pump lasers from the excited states [21,22]. We have explained the step-by-step procedure to obtain the

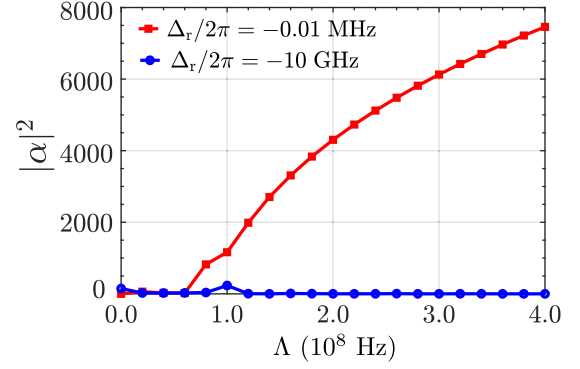


FIG. 3. The intracavity photon numbers $|\alpha|^2$ versus incoherent pumping Λ for $\Omega_c/2\pi = -800$ MHz with small ($\Delta_{r,s,e}/2\pi = -0.01$ MHz) and very large detuning values ($\Delta_{r,s,e}/2\pi = -10$ GHz). The dephasing rate for this plot is $\gamma_{ph} = 0$, cavity decay $\kappa/2\pi = 0.02$ MHz, spontaneous decay $\gamma/2\pi = 2.6$ MHz and atom-cavity coupling $\eta/2\pi = 50$ MHz.

reduced Hamiltonian where the excited states $|e\rangle$, $|r\rangle$, and $|s\rangle$ are adiabatically eliminated in Appendix B. We use the Schrödinger equation to find the evolution of the state and then calculate equation of motion of the coefficients involved with each state of the atom [20]. Considering Eq. (10) and assuming $\frac{\Omega_c}{\Delta_r \Delta_e} \ll 1$, we arrive at the two-level Hamiltonian, [rewriting Eq. (B12)],

$$\hat{H}_{red} = \omega_0 \hat{J}_z + \omega_c \hat{a}^\dagger \hat{a} + \frac{G}{\sqrt{N}} (\hat{a}^\dagger + \hat{a}) (\hat{J}_+ + \hat{J}_-), \quad (11)$$

where $\hat{J}_z = \sum_i \hat{\sigma}_{z(i)}$, $\hat{J}_+ = \sum_i \hat{\sigma}_{+(i)}$ and $\hat{J}_- = \sum_i \hat{\sigma}_{-(i)}$, $\omega_0 = \Delta_g - \frac{\Omega_1^2}{\Delta_r} + \frac{\Omega_2^2}{\Delta_e}$, $\omega_c = \Delta_{cav} - (\frac{\eta_c^2}{\Delta_e} + \frac{\eta_r^2}{\Delta_r})$ and $G = -\frac{\sqrt{N} \eta_r \Omega_1}{\Delta_r} = -\frac{\sqrt{N} \eta_e \Omega_2}{\Delta_e}$. The values taken for the numerical simulation satisfy the conditions necessary to obtain the Hamiltonian in Eq. (11). To exemplify we consider $\Delta_r/2\pi = -10.0$ GHz, $\Delta_s/2\pi = -10.0$ GHz, $\Delta_e/2\pi = -10.0$ GHz, $\Omega_c/2\pi = -800$ MHz and the other parameters are same as in Sec. IV A. For these large detunings values, $|\alpha|^2$ becomes zero though Λ value increases and $\Omega_c/2\pi = -800$ MHz (Fig. 3). It indicates that Ω_c and Λ has no impact on the system with very large detuning as the excited states are adiabatically eliminated.

C. Decoherence effect

Next, we explore the effect of dephasing γ_{ph} in our model, we show the variation of $|\alpha|^2$ with incoherent pumping Λ taking $\gamma_{ph}/2\pi = \{0, 390, 740\}$ MHz. The detuning values are $\Delta_s = \Delta_g = \Delta_e = \Delta_r = -0.01 \times 2\pi$ MHz. The coherent pumping $\Omega_c/2\pi = -800$ MHz and the other parameters are same in Sec. IV A. The average photon numbers reduces with increase in dephasing albeit it is to be noted that Ω_c still has an impact on the system (Fig. 4). We can observe that for very large dephasing value, $|\alpha|^2$ does not go to zero and thus conclude that the system is robust against decoherence. This type of effect has also been seen earlier in optics and plasmonic studies [27,49].

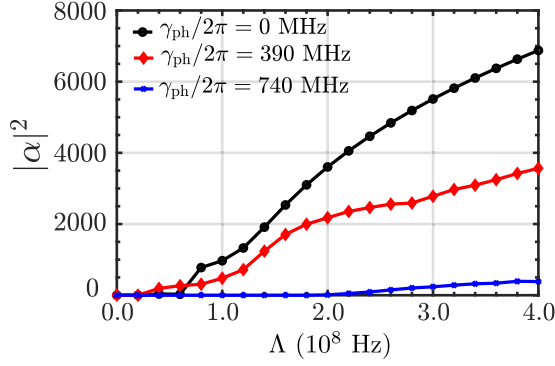


FIG. 4. The effect of different dephasing values $\gamma_{\text{ph}}/2\pi = \{0, 390, 740\}$ MHz is studied on the intracavity photon numbers $|\alpha|^2$ versus incoherent coupling Λ . As γ_{ph} increases $|\alpha|^2$ decreases, but it is observed that the effect of coherent field $\tilde{\Omega}_c/2\pi = -800$ MHz is still retained even for very large dephasing value. The cavity decay is $\kappa/2\pi = 0.02$ MHz, spontaneous decay $\gamma/2\pi = 2.6$ MHz and atom-cavity coupling $\eta/2\pi = 50$ MHz.

D. Variation with atoms

In this paper, we have discussed the effect of coherent and incoherent pumping on the photon numbers for $N = 100$ atoms. In addition to the case $N = 100$, we also analysed a scenario corresponding to a small number of atoms, i.e., $N = 8$ to check whether the model still prevails. The parameters used are same as in Sec. IV A. The magnitude of intracavity photon numbers $|\alpha|^2$ is less for $N = 8$ atoms in comparison to $N = 100$ but the quantum coherence effect of $\tilde{\Omega}_c$ is robust [Fig. 5(a)]. The influence of $\tilde{\Omega}_c/2\pi = -800$ MHz is very pronounced, but $\tilde{\Omega}_1 < \tilde{\Omega}_c < \tilde{\Omega}_2$, i.e., $\tilde{\Omega}_c/2\pi = -500$ MHz still has an effect more than $\tilde{\Omega}_c = 0$. For large $\tilde{\Omega}_c$, i.e., $\tilde{\Omega}_c/2\pi = -800$ MHz, the number of photons increases with increasing atoms [Fig. 5(b)].

V. TRANSIENT ANALYSIS

Here we study the time evolution of the intracavity photon number $|\alpha|^2$ for resonant detuning ($\Delta_x = 0$, $x = e, s, g, r$) and off-resonant detuning ($\Delta_x/2\pi = -0.01$ MHz) cases. The

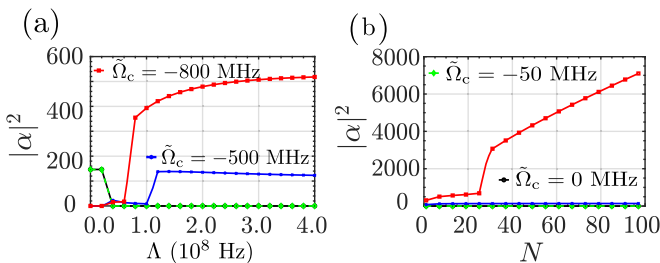


FIG. 5. Effect of the number of atoms on intracavity photon numbers $|\alpha|^2$ is studied for different values of coherent coupling $\tilde{\Omega}_c = \tilde{\Omega}_c/2\pi$ and $\Lambda = 0.4$ GHz. (a) for number of atom $N = 8$. The quantum coherence effect is robust for even such a small number of atoms. (b) variation of $|\alpha|^2$ with N for different values of coherent pumping $\tilde{\Omega}_c/2\pi$. Like previous case, here too cavity coupling $\eta/2\pi = 50$ MHz, dephasing rate is $\gamma_{\text{ph}} = 0$, cavity decay $\kappa/2\pi = 0.02$ MHz and spontaneous decay $\gamma/2\pi = 2.6$ MHz.

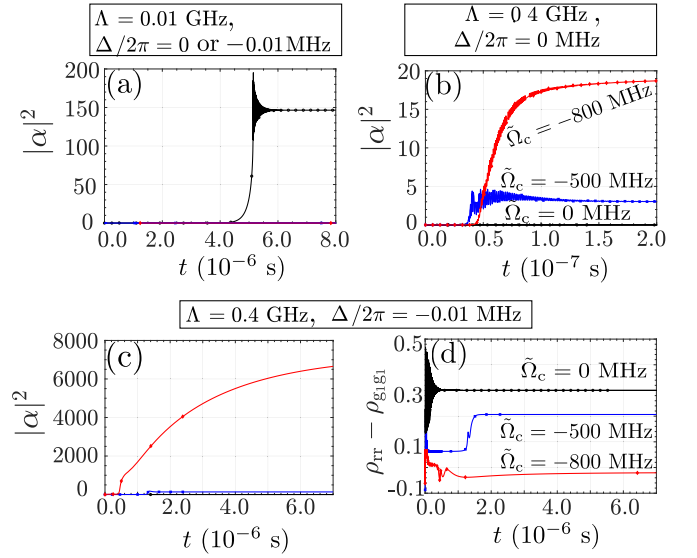


FIG. 6. Time evolution of photon numbers $|\alpha|^2$ is shown for different values of incoherent pumping Λ , coherent pumping $\tilde{\Omega}_c = \tilde{\Omega}_c/2\pi$, and detunings. (a) For both $\Delta_{r,s,g,e} = 0$ and $\Delta_{r,s,g,e}/2\pi = -0.01$ MHz, and $\Lambda = 0.01$ GHz; $\tilde{\Omega}_c/2\pi = \{-500, -800\}$ MHz always have a zero steady-state value while $\tilde{\Omega}_c/2\pi = 0$ reaches a finite value of steady state. (b) For $\Lambda = 0.4$ GHz and $\Delta_{r,s,g,e} = 0$, $\tilde{\Omega}_c/2\pi = -800$ MHz reaches finite steady state earlier. (c) For $\Lambda = 0.4$ GHz and $\Delta_{r,s,g,e}/2\pi = -0.01$ MHz, $\tilde{\Omega}_c/2\pi = -800$ MHz reaches around $6.4 \mu\text{s}$. (d) Time evolution of population inversion $\rho_{\text{tr}} - \rho_{g_1g_1}$ is shown for $\Lambda/2\pi = 0.4$ GHz and $\Delta_{r,s,g,e}/2\pi = -0.01$ MHz. For all figures $\gamma_{\text{ph}} = 0$, cavity decay $\kappa/2\pi = 0.02$ MHz, spontaneous decay $\gamma/2\pi = 2.6$ MHz, atom-cavity coupling $\eta/2\pi = 50$ MHz, and $N = 100$ atoms.

effect of coherent laser field and incoherent pumping on transient response of the system is also explored using $\tilde{\Omega}_c/2\pi = \{0, -500, -800\}$ MHz and $\Lambda = \{0.01, 0.4\}$ GHz, respectively. The cavity field is considered to be in resonance with the laser pump frequencies, i.e., $\Delta_{\text{cav}} = 0$ [17,34].

For $\Lambda = 0.01$ GHz, for both zero and small detuning values, $|\alpha|^2$ increases with time and reaches a finite steady-state value at $t \sim 6.5 \mu\text{s}$ for $\tilde{\Omega}_c = 0$ [Fig. 6(a)]. The system is at a zero steady state almost at similar time for $\tilde{\Omega}_c/2\pi = \{-500, -800\}$ MHz [Fig. 6(a)]. Considering the value $\Lambda = 0.4$ GHz, a finite steady state is reached at an earlier instant $t \sim 0.15 \mu\text{s}$ for $\tilde{\Omega}_c/2\pi = \{-500, -800\}$ MHz [Fig. 6(b)].

With a small detuning and $\Lambda = 0.4$ GHz, the magnitude of $|\alpha|^2$ increases manifold as we increase the values of $\tilde{\Omega}_c$ [Fig. 6(c)] because of the quantum coherence effect as explained earlier. The steady state for $\tilde{\Omega}_c/2\pi = -800$ MHz, which is actually a large value of $|\alpha|^2$ is attained earlier than the case with small incoherent drive and $\tilde{\Omega}_c/2\pi = 0$ MHz [Fig. 6(a)], but later than large incoherent drive and zero detuning [Fig. 6(b)]. This concludes that we can achieve such large steady-state value for large incoherent pumping and coherent drive at not much expense of time.

We have also studied the transient response of population inversion in the states $|g_1\rangle \rightarrow |r\rangle$ [Fig. 6(d)]. For large coherent pumping ($\tilde{\Omega}_c/2\pi = -800$ MHz), the population inversion reaches the steady state earlier than $|\alpha|^2$. Therefore, it can be

concluded that different parameters in this system may reach the steady at different instant depending on the coherent drive.

VI. QUANTUM DYNAMICS

Till now, we have observed the semiclassical behavior of the proposed system. The observations are valid if the underlying semiclassical approximation related to the factorization of the mean values of the operators are satisfied, and quantum fluctuations are ignored (Sec. III). In order to determine whether this system actually portrays the profound effects, here we have simulated the full quantum dynamics of the proposed system.

The Liouville space dimension corresponding to N l -level atom is l^{2N} , leading to a computationally impossible scenario for even small value of l and N [36,50]. In such cases, we can use QUTIP, which is favorable for finding quantum dynamics of large two-level system using quantum symmetry [36,51] or PSQUASP, which also provides a suitable platform for the study of two-level as well as multilevel systems interacting with bosonic fields and laser fields by the reducing the computational expense using the permutation symmetry [50,52].

We have developed a five-level ($l = 5$) full quantum model of the proposed system in the framework of PSQUASP. Appendix C provides details of the numerical implementation, which involves the incorporation of the permutation symmetry in the master equation symmetry in the master equation [Eqs. (C5) to (C9)] and visualization of the elements of the master equation using graph theory (Figs. 8–11). These sketches are then directly translated into code.

We limit our quantum simulation to two atoms ($N = 2$) as the number of photon Fock state required for our system is quite high, which increases the Hilbert space dimension. Figure 7 presents the result of the transient analysis. The intracavity photon numbers $|\alpha|^2$ increases with time and reaches a steady state in about 5–7 μ s. It is also observed that $|\alpha|^2$ increases with the photon Fock state (M) and finally converges at $M \approx 900$. However, the semiclassical solution of the system (with $N = 2$ and keeping the same system parameters) shows

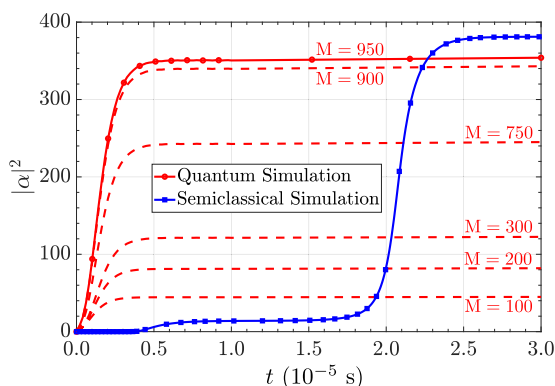


FIG. 7. Transient analysis of photon numbers $|\alpha|^2$ for both semiclassical and quantum simulation are shown in this figure. The coherent pumping values are $\Omega_c/2\pi = -800$ MHz, $\Omega_1/2\pi = -470$ MHz, $\Omega_2/2\pi = -780$ MHz and incoherent pumping $\Lambda = 0.4$ GHz. The quantum simulation nearly converges when the photon Fock state $M \approx 900$.

that the steady state reaches around 25 μ s (Fig. 7). Albeit the differences in the evolution of the system studied using full quantum dynamics and its semiclassical approximation, they provide an almost agreeable steady-state intracavity photon number.

In this work, we have studied the proposed system in the strong-coupling regime ($\eta/2\pi = 50$ MHz), where the quantum dynamics simulation converges for large photon Fock states M . However, in the weak-coupling regime (i.e., $\eta \ll \gamma, \kappa$) the full quantum model requires considerably smaller $M \approx 10$ –20 and the result matches with the semiclassical solution where $|\alpha|^2$ is negligible (not shown in the figure). It is also observed from the semiclassical and the full quantum simulation that the quantum coherence effect is significant in the strong-coupling regime only.

VII. CONCLUSION

In this paper, we have proposed a multilevel open cavity QED system considering coherent and incoherent pumping effects. In the presence of small detunings, the intracavity photon numbers increase multifold owing to quantum coherence effects in the fifth energy level of the atom. Strikingly, this enhancement with the coherent and incoherent pumping comes with no population inversion. These characteristics even hold for a small number of atoms as well. However, when the detunings are very large, adiabatic elimination of the excited states is possible, and consequently, even a high level of coherent pumping has negligible influence on the system. When adiabatic elimination is allowed, we have effectively reduced the system to an equivalent two-level system. A transient analysis shows that the system attains steady state at an earlier instant when the incoherent coupling is larger. It can also be seen that different system parameter reaches steady state at different instant of time. An exact, full quantum dynamics simulation of the system shows an almost agreeable steady-state solution when compared to the semiclassical analysis for $N = 2$ atoms. The proposed model can be applied to other theoretical and experimental setups of cavity QED system [24,26,53]. The application of additional coherent field, as proposed in this study, can also be achieved in QED chemistry [54,55], circuit QED [13], etc. Moreover, the observations made in this paper can be useful in enhancing the control drive of nanostructure systems [56–58] and synthesizing different models for further controllable optical effects [59].

ACKNOWLEDGMENTS

A.D. would like to thank Dr. S Parkins (University of Auckland), Dr. T. Warnakula, R. T. Wijesekara, Dr. L. Kumarapperuma for the helpful discussions and all members of A χ L at Monash University for their encouragement and support. The work of A.D. is supported by the Monash University Institute of Graduate Research.

APPENDIX A: DERIVATION OF MASTER EQUATION

The detailed derivation of the master equation is given in Ref. [42]. Here, we provide an outline of this derivation in our notation to enhance the readability of this paper. Let \mathcal{H}_S be the Hilbert space of the system S and \mathcal{H}_B the Hilbert space of

the environment B . Interaction between them results a change in the system as well as due to internal dynamics of S . The resulting Hamiltonian \mathcal{H} is of the form

$$\mathcal{H} = \mathcal{H}_s + \mathcal{H}_B + \mathcal{H}_I(t), \quad (\text{A1})$$

where $\mathcal{H}_I(t)$ is the interaction Hamiltonian between S and B . We are particularly interested in the dynamics of subsystem S . To understand the dynamics let us begin with the von Neumann equation in the interaction picture

$$\dot{\hat{\rho}}(t) = -i[\mathcal{H}_I(t), \hat{\rho}(t)]. \quad (\text{A2})$$

The integral form of $\hat{\rho}(t)$, which is the density matrix is given by:

$$\hat{\rho}(t) = \hat{\rho}(0) - i \int_0^t ds [\mathcal{H}_I(s), \hat{\rho}(s)]. \quad (\text{A3})$$

Putting Eq. (A3) back into Eq. (A2) and tracing over B we get,

$$\dot{\hat{\rho}}(t) = - \int_0^t ds \text{tr}_B [\mathcal{H}_I(t), [\mathcal{H}_I(s), \hat{\rho}(s)]], \quad (\text{A4})$$

with the assumption that $\text{tr}_B[\mathcal{H}_I(t), \hat{\rho}(0)] = 0$. As the right-hand side of Eq. (A4) still has $\hat{\rho}(s)$, we use the Born approximation, which considers that the interaction has no significant affect on $\hat{\rho}_B$ (reservoir density matrix). Thus, we use the following tensor product to represent the total system at any given time t :

$$\hat{\rho}(t) \approx \hat{\rho}_s(t) \otimes \hat{\rho}_B. \quad (\text{A5})$$

Substituting Eq. (A5) into Eq. (A4) we get a integrodifferential equation,

$$\dot{\hat{\rho}}_s(t) = - \int_0^t ds \text{tr}_B [\mathcal{H}_I(t), [\mathcal{H}_I(s), \hat{\rho}_s(s) \otimes \hat{\rho}_B]]. \quad (\text{A6})$$

Considering the Markovian approximation one can obtain,

$$\dot{\hat{\rho}}_s(t) = - \int_0^\infty ds \text{tr}_B [\mathcal{H}_I(t), [\mathcal{H}_I(t-s), \hat{\rho}_s(t) \otimes \hat{\rho}_B]]. \quad (\text{A7})$$

Let us write \mathcal{H}_I in the Schrödinger picture as,

$$\mathcal{H}_I = \sum_\alpha A_\alpha \otimes B_\alpha \quad (\text{A8})$$

with symmetric operators A_α and B_α . In the next step we decompose \mathcal{H}_I into eigenoperators of the system Hamiltonian \mathcal{H}_s as,

$$\begin{aligned} \mathcal{H}_I(t) &= \sum_{\alpha, \omega} e^{-i\omega t} A_\alpha(\omega) \otimes B_\alpha(t), \\ A_\alpha(\omega) &:= \sum_{\omega=\lambda-\lambda'} \mathcal{Q}(\lambda) A_\alpha \mathcal{Q}(\lambda'), \end{aligned} \quad (\text{A9})$$

with eigenspace $\mathcal{Q}(\lambda)$ for energy eigenvalue λ ; ω is the fixed energy difference between the energy eigenvalues λ and λ' . Also, $B_\alpha(t) = e^{i\mathcal{H}_B t} B_\alpha e^{-i\mathcal{H}_B t}$.

Substituting Eq. (A9) into Eq. (A7) and we get,

$$\begin{aligned} \dot{\hat{\rho}}_s(t) &= \sum_{\omega, \omega'} \sum_{\alpha, \beta} e^{i(\omega' - \omega)t} \Gamma_{\alpha\beta}(\omega) (A_\beta(\omega) \hat{\rho}_s(t) A_\alpha^\dagger(\omega') \\ &\quad - A_\alpha^\dagger(\omega') A_\beta(\omega) \hat{\rho}_s(t)) + \text{H.c.} \end{aligned} \quad (\text{A10})$$

Here, $\Gamma_{\alpha\beta}(\omega) = \int_0^\infty ds e^{i\omega s} \langle B_\alpha^\dagger(t) B_\beta(t-s) \rangle$.

Considering the rotating-wave approximation (neglecting the nonsecular terms for which $\omega' \neq \omega$) in Eq. (A10) we have,

$$\dot{\hat{\rho}}(t) = -i[\mathcal{H}_s, \hat{\rho}(t)] + \sum \frac{\gamma_\downarrow}{2} \mathcal{L}_{J_{-,n}}[\hat{\rho}_s] + \sum \frac{\gamma_\uparrow}{2} \mathcal{L}_{J_{+,n}}[\hat{\rho}_s], \quad (\text{A11})$$

with

$$\begin{aligned} \mathcal{L}_{J_{-,n}}[\hat{\rho}_s] &= A(\omega) \hat{\rho}(t) A^\dagger(\omega) - \frac{1}{2} \{A^\dagger(\omega) A(\omega), \hat{\rho}(t)\}, \\ \mathcal{L}_{J_{+,n}}[\hat{\rho}_s] &= A^\dagger(\omega) \hat{\rho}(t) A(\omega) - \frac{1}{2} \{A(\omega) A^\dagger(\omega), \hat{\rho}(t)\}. \end{aligned} \quad (\text{A12})$$

The coefficient of decay rates and coefficient of pumping gains are given by γ_\downarrow and γ_\uparrow , respectively. Eq. (A11) presents the master equation considered in this work.

$\mathcal{L}[\hat{\rho}]$ is the Liouvillian superoperator. It is defined by $\mathcal{L}_c[\hat{\rho}] = 2\hat{c}\hat{\rho}\hat{c}^\dagger - \hat{c}^\dagger\hat{c}\hat{\rho} - \hat{\rho}\hat{c}^\dagger\hat{c}$ for any operator \hat{c} and it includes the non-Hamiltonian dynamics into the system. The Lindblad term for the collective spontaneous transition of the atom decay rate γ_\downarrow [44],

$$\mathcal{L}_{\text{spon}}[\hat{\rho}_s] = \frac{\gamma_\downarrow}{2} \sum_{j=1}^N (2\hat{J}_j^- \hat{\rho} \hat{J}_j^+ - \hat{J}_j^+ \hat{J}_j^- \hat{\rho} - \hat{\rho} \hat{J}_j^+ \hat{J}_j^-), \quad (\text{A13})$$

The collective \hat{J} operators are defined as $\hat{J}^- = \sum_n^N \hat{\sigma}_n^-$ and $\hat{J}^+ = \sum_n^N \hat{\sigma}_n^+$. Each σ operators are given by, $\hat{\sigma}_{ik}^{(-)} = |i\rangle\langle k|$ and $\hat{\sigma}_{ik}^{(+)} = |k\rangle\langle i|$ with $i, k \in \{g_1, g_2, r, e, s\}$ being the transition states of the atom. Now, for simplicity, we consider spontaneous emission from these states $|r\rangle \rightarrow |g_1\rangle$, $|s\rangle \rightarrow |g_1\rangle$, $|s\rangle \rightarrow |r\rangle$, and $|e\rangle \rightarrow |g_2\rangle$. Expanding the Lindblad operator for the spontaneous decay in our case,

$$\begin{aligned} \frac{\gamma_\downarrow}{2} \mathcal{L}_{\text{spon}}[\hat{\rho}_s] &= \sum_{j=1}^N \left[\frac{\gamma_{\text{sr}}}{2} (2\hat{J}_{\text{rs}}^j \hat{\rho} \hat{J}_{\text{sr}}^j - \hat{J}_{\text{sr}}^j \hat{J}_{\text{rs}}^j \hat{\rho} - \hat{\rho} \hat{J}_{\text{sr}}^j \hat{J}_{\text{rs}}^j) \right. \\ &\quad + \frac{\gamma_{\text{rg}}}{2} (2\hat{J}_{\text{g}_1\text{r}}^j \hat{\rho} \hat{J}_{\text{rg}}^j - \hat{J}_{\text{rg}}^j \hat{J}_{\text{g}_1\text{r}}^j \hat{\rho} - \hat{\rho} \hat{J}_{\text{rg}}^j \hat{J}_{\text{g}_1\text{r}}^j) \\ &\quad + \frac{\gamma_{\text{eg}}}{2} (2\hat{J}_{\text{g}_2\text{e}}^j \hat{\rho} \hat{J}_{\text{eg}}^j - \hat{J}_{\text{eg}}^j \hat{J}_{\text{g}_2\text{e}}^j \hat{\rho} - \hat{\rho} \hat{J}_{\text{eg}}^j \hat{J}_{\text{g}_2\text{e}}^j) \\ &\quad \left. + \frac{\gamma_{\text{sg}}}{2} (2\hat{J}_{\text{g}_1\text{s}}^j \hat{\rho} \hat{J}_{\text{sg}}^j - \hat{J}_{\text{sg}}^j \hat{J}_{\text{g}_1\text{s}}^j \hat{\rho} - \hat{\rho} \hat{J}_{\text{sg}}^j \hat{J}_{\text{g}_1\text{s}}^j) \right]. \end{aligned} \quad (\text{A14})$$

We do not consider the cross spontaneous decay, i.e., decay from the excited state $|r\rangle$ ($|e\rangle$) to the ground state $|g_2\rangle$ ($|g_1\rangle$). The addition of the cross decay channels terms and the dipole-forbidden relaxation rates has a negligible effect in the parameter regime considered [48]. They result in a very slight reduction in the amplitude of intracavity photons [31,60]. Therefore, such terms can be neglected to simplify the model.

The Lindblad term related to the pumping of the atom is similar with Eq. (A13) but with the substitution of $\gamma_\downarrow \rightarrow \gamma_\uparrow$, $\hat{J}_j^+ \rightarrow \hat{J}_j^-$ and $\hat{J}_j^- \rightarrow \hat{J}_j^+$,

$$\mathcal{L}_{\text{pump}}[\hat{\rho}_s] = \frac{\gamma_\uparrow}{2} \sum_{j=1}^N (2\hat{J}_j^+ \hat{\rho} \hat{J}_j^- - \hat{J}_j^- \hat{J}_j^+ \hat{\rho} - \hat{\rho} \hat{J}_j^- \hat{J}_j^+). \quad (\text{A15})$$

In our model, we consider the pumping from $|g_1\rangle \rightarrow |s\rangle$, therefore,

$$\frac{\gamma_{\uparrow}}{2} \mathcal{L}_{\text{pump}}[\hat{\rho}_s] = \sum_{j=1}^N \frac{\Lambda}{2} (2\hat{f}_{sg_1}^j \hat{\rho} \hat{f}_{g_1s}^j - \hat{f}_{g_1s}^j \hat{f}_{sg_1}^j \hat{\rho} - \hat{\rho} \hat{f}_{g_1s}^j \hat{f}_{sg_1}^j). \quad (\text{A16})$$

Similarly, Lindblad term for cavity decay can be written as,

$$\mathcal{L}_{\text{cav}}[\hat{\rho}_s] = -\frac{\kappa}{2} (\hat{a}^\dagger \hat{a} \hat{\rho} + \hat{\rho} \hat{a}^\dagger \hat{a} - 2\hat{a} \hat{\rho} \hat{a}^\dagger). \quad (\text{A17})$$

APPENDIX B: REDUCED HAMILTONIAN AFTER ADIABATIC ELIMINATION

To obtain the reduced Hamiltonian we introduce the state vector $|\Psi(t)\rangle$, which can be defined as [20,25]:

$$|\Psi(t)\rangle = \sum_{m=0}^{\infty} [(b_r^m |r\rangle + b_e^m |e\rangle + b_s^m |s\rangle + b_{g_1}^m |g_1\rangle + b_{g_2}^m |g_2\rangle) \otimes |m\rangle]. \quad (\text{B1})$$

Here, $|m\rangle$ is cavity-mode state and the coefficients b_r^m , b_e^m , b_s^m , $b_{g_1}^m$, and $b_{g_2}^m$ are time dependent. Substituting Eq. (B1) and Eq. (4) into the Schrödinger equation Eq. (B2),

$$i \frac{d|\Psi(t)\rangle}{dt} = \frac{1}{\hbar} \hat{H}_{\text{in}} |\Psi\rangle. \quad (\text{B2})$$

Next we get the equation of motion for b_r^m , b_e^m , b_s^m , $b_{g_1}^m$, and $b_{g_2}^m$,

$$i\dot{b}_r^m = \Delta_r b_r^m + (\Omega_1 b_{g_2}^m + \eta_r b_{g_1}^{m+1} \sqrt{m+1}) e^{ikx} + \Omega_c b_s^m e^{-ikx}, \quad (\text{B3a})$$

$$i\dot{b}_e^m = \Delta_e b_e^m + (\Omega_2 b_{g_1}^m + \eta_e b_{g_2}^{m+1} \sqrt{m+1}) e^{ikx}, \quad (\text{B3b})$$

$$i\dot{b}_s^m = \Delta_s b_s^m + \Omega_c b_r^m e^{ikx}, \quad (\text{B3c})$$

$$i\dot{b}_{g_2}^m = \Delta_g b_{g_2}^m + (\Omega_1 b_r^m + \eta_e b_e^{m-1} \sqrt{m}) e^{-ikx}, \quad (\text{B3d})$$

$$i\dot{b}_{g_1}^m = (\Omega_2 b_e^m + \eta_r b_r^{m-1} \sqrt{m}) e^{-ikx}, \quad (\text{B3e})$$

the term $\Delta_{\text{cav}} \hat{a}^\dagger \hat{a}$ is neglected in Eq. (4) to arrive at the above equations. This term will be added later on. Using $\Delta_s, \Delta_r, \Delta_e \gg \{\Omega_{1,2,c}, \eta_{r,e}\}$, the excited states $|r\rangle$, $|e\rangle$, and $|s\rangle$ can be adiabatically eliminated. b_r^m , b_e^m , and b_s^m goes to zero on long timescale, therefore Eq. (B3a), Eq. (B3b), and Eq. (B3c) can be written as:

$$b_r^m = -\frac{e^{ikx}}{\Delta_r} (\Omega_1 b_{g_2}^m + \eta_r b_{g_1}^{m+1} \sqrt{m+1}) + \frac{e^{-ikx}}{\Delta_r} \Omega_c b_s^m, \quad (\text{B4a})$$

$$b_e^m = -\frac{e^{ikx}}{\Delta_e} (\Omega_2 b_{g_1}^m + \eta_e b_{g_2}^{m+1} \sqrt{m+1}), \quad (\text{B4b})$$

$$b_s^m = -\frac{e^{ikx}}{\Delta_s} \Omega_c b_r^m. \quad (\text{B4c})$$

Putting Eq. (B4c) in Eq. (B4a), and using the condition that $\frac{\Omega_c^2}{\Delta_r \Delta_s} \ll 1$, the resulting expressions for b_r^m and b_e^m can be substituted in Eq. (B3d) and Eq. (B3e) to get,

$$i\dot{b}_{g_2}^m = \left(\Delta_g - \frac{\Omega_1^2}{\Delta_r} \right) b_{g_2}^m - \frac{\eta_r \Omega_1}{\Delta_r} \sqrt{m+1} b_{g_1}^{m+1} - \frac{\eta_e \Omega_2}{\Delta_e} \sqrt{m} b_{g_1}^{m-1} - \frac{\eta_r^2}{\Delta_e} b_{g_2}^m m, \quad (\text{B5a})$$

$$i\dot{b}_{g_1}^m = -\frac{\Omega_2^2}{\Delta_e} b_{g_1}^m - \frac{\eta_e \Omega_2}{\Delta_e} \sqrt{m+1} b_{g_2}^{m+1} - \frac{\eta_r \Omega_1}{\Delta_r} \sqrt{m} b_{g_2}^{m-1} - \frac{\eta_r^2}{\Delta_r} b_{g_1}^m m. \quad (\text{B5b})$$

The reduced Hamiltonian with only the ground states $|g_1\rangle$ and $|g_2\rangle$ can be therefore written as,

$$\hat{H}_{\text{red}} = \left(\Delta_g - \frac{\Omega_1^2}{\Delta_r} \right) |g_2\rangle \langle g_2| - \frac{\eta_r \Omega_1}{\Delta_r} (\hat{\sigma}_+ \hat{a} + \hat{\sigma}_- \hat{a}^\dagger) - \frac{\eta_e \Omega_2}{\Delta_e} (\hat{\sigma}_- \hat{a} + \hat{\sigma}_+ \hat{a}^\dagger) - \frac{\Omega_2^2}{\Delta_e} |g_1\rangle \langle g_1| - \frac{\eta_e^2}{\Delta_e} \hat{a}^\dagger \hat{a} |g_2\rangle \langle g_2| - \frac{\eta_r^2}{\Delta_r} \hat{a}^\dagger \hat{a} |g_1\rangle \langle g_1|, \quad (\text{B6})$$

where,

$$\hat{\sigma}_+ = |g_2\rangle \langle g_1|, \quad \hat{\sigma}_- = |g_1\rangle \langle g_2|. \quad (\text{B7})$$

We can redefine $|g_2\rangle \langle g_2|$ and $|g_1\rangle \langle g_1|$ in Eq. (B6) with $\hat{\sigma}_z$ and $\mathbf{1}$,

$$|g_2\rangle \langle g_2| = \frac{\mathbf{1} + \hat{\sigma}_z}{2}, \quad |g_1\rangle \langle g_1| = \frac{\mathbf{1} - \hat{\sigma}_z}{2}. \quad (\text{B8})$$

To arrive at a neat and simple Hamiltonian we neglect the constant terms in Eq. (B6),

$$\hat{H}_{\text{red}} = \omega_0 \frac{\hat{\sigma}_z}{2} + \omega_c \hat{a}^\dagger \hat{a} + g_r (\hat{\sigma}_+ \hat{a} + \hat{\sigma}_- \hat{a}^\dagger) + g_e (\hat{\sigma}_- \hat{a} + \hat{\sigma}_+ \hat{a}^\dagger) + \Gamma \hat{a}^\dagger \hat{a} \frac{\hat{\sigma}_z}{2} \quad (\text{B9})$$

where,

$$\omega_0 = \Delta_g - \frac{\Omega_1^2}{\Delta_r} + \frac{\Omega_2^2}{\Delta_e}, \quad (\text{B10a})$$

$$\omega_c = \Delta_{\text{cav}} - \left(\frac{\eta_e^2}{\Delta_e} + \frac{\eta_r^2}{\Delta_r} \right), \quad (\text{B10b})$$

$$g_r = -\frac{\eta_r \Omega_1}{\Delta_r}, \quad (\text{B10c})$$

$$g_e = -\frac{\eta_e \Omega_2}{\Delta_e}, \quad (\text{B10d})$$

$$\Gamma = \frac{\eta_r^2}{\Delta_r} - \frac{\eta_e^2}{\Delta_e}. \quad (\text{B10e})$$

Putting $\frac{\eta_r^2}{\Delta_r} = \frac{\eta_e^2}{\Delta_e}$, we get the two-level Hamiltonian,

$$\hat{H}_{\text{red}} = \omega_0 \hat{\sigma}_z / 2 + \omega_c \hat{a}^\dagger \hat{a} + g_r (\hat{\sigma}_+ \hat{a} + \hat{\sigma}_- \hat{a}^\dagger) + g_e (\hat{\sigma}_- \hat{a} + \hat{\sigma}_+ \hat{a}^\dagger). \quad (\text{B11})$$

Further considering $g_r = g_e$, we obtain the Dicke model with the counterrotating term for N number of atoms,

$$\hat{H}_{\text{red}} = \omega_0 \hat{J}_z + \omega_c \hat{a}^\dagger \hat{a} + \frac{G}{\sqrt{N}} (\hat{a}^\dagger + \hat{a}) (\hat{J}_+ + \hat{J}_-), \quad (\text{B12})$$

where $G = -\frac{\sqrt{N} \eta_r \Omega_1}{\Delta_r} = -\frac{\sqrt{N} \eta_e \Omega_2}{\Delta_e}$, $\hat{J}_z = \sum_i^N \hat{\sigma}_{z(i)}$, $\hat{J}_+ = \sum_i^N \hat{\sigma}_{+(i)}$ and $\hat{J}_- = \sum_i^N \hat{\sigma}_{-(i)}$.

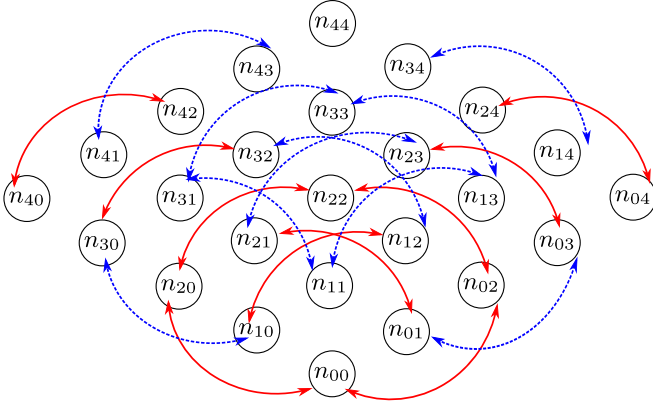


FIG. 8. Interaction of the cavity and atom: densities are exchanged between: n_{22} & n_{00} (red solid lines) as well as n_{33} and n_{31} (blue dashed lines) via the build up of quantum coherence. This graph corresponds to the Lindblad equation given in Eq. (C5) and Eq. (C6). Sketch of the actions of the different contributions of the Lindblad equation. Arrows pointing from circle A to circle B correspond to a build up of density matrix entries with higher number in B and lower number in A.

APPENDIX C: SETUP FOR FIVE-LEVEL SYSTEM IN PSQUASP

In this Appendix we provide the details of constructing the density matrix equation of our five-level system for PSQUASP. For our convenience we rename each state in Fig. 1 as $|g_1\rangle \rightarrow |0\rangle$, $|g_2\rangle \rightarrow |1\rangle$, $|r\rangle \rightarrow |2\rangle$, $|e\rangle \rightarrow |3\rangle$, and $|s\rangle \rightarrow |4\rangle$. For $(d+1)$ level systems where $d = l - 1$, the permutationally symmetrized Liouvillian states are,

$$\hat{\mathcal{P}}[\{n_{ij}\}] = s \otimes_{i,j=0}^d \hat{\sigma}_{ij}^{\otimes n_{ij}}, \quad (\text{C1})$$

where $\{n_{ij}\} = \{n_{dd}, n_{d(d-1)}, \dots\}$ is the set of all numbers n_{ij} . The product in Eq. (C1) consists of N individual spin matrices, one for each multilevel system. S is the symmetrization operator. Looking at the time evolution of the respective density matrix elements,

$$\text{tr}[\hat{\mathcal{P}}[\{n_{ij}\}]\hat{\rho}] = \mathcal{P}[\{n_{ij}\}], \quad (\text{C2})$$

we get the different contributions of the Hamiltonian. We start by writing the equations of motion for the density matrix

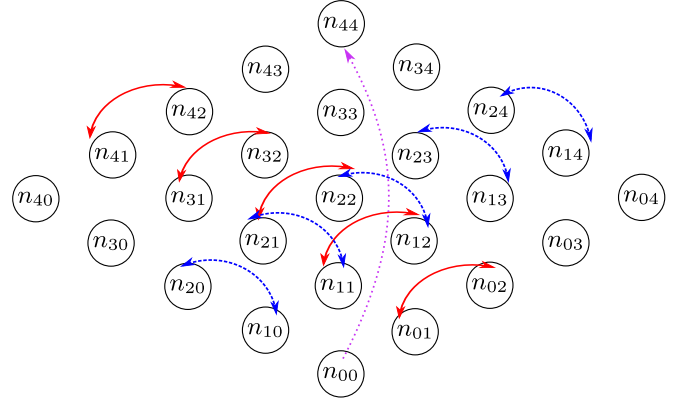


FIG. 9. Contribution of optical pumping of the system Ω_1 ; densities are exchanged between n_{22} and n_{11} (red solid lines and blue dashed lines) via the buildup of quantum coherence. This graph corresponds to the Lindblad equation given in Eq. (C7). Action of the Lindblad dissipators : incoherent pumping is given by purple (dotted) arrows.

associated to Eq. (6),

$$\begin{aligned} \hat{\rho}_{\text{int}} = & \frac{i}{\hbar} [\hat{\rho}_s, H_{\text{CA}} + H_{\text{LA}}] + \mathcal{L}[J_{02}]\hat{\rho}_s + \mathcal{L}[J_{04}]\hat{\rho}_s \\ & + \mathcal{L}[J_{13}]\hat{\rho}_s + \mathcal{L}[J_{34}]\hat{\rho}_s + \mathcal{L}[J_{40}]\hat{\rho}_s. \end{aligned} \quad (\text{C3})$$

The set of elements required to form the permutationally symmetrized Liouvillian states as in Eq. (C1) are,

$$\begin{aligned} \mathcal{P}[n_{44}, n_{43}, n_{42}, n_{41}, n_{40}, n_{34}, n_{33}, n_{32}, n_{31}, n_{30}, \\ n_{24}, n_{23}, n_{22}, n_{21}, n_{20}, n_{14}, n_{13}, n_{12}, n_{11}, n_{10}, n_{04}, \\ n_{03}, n_{02}, n_{01}; k, p], \end{aligned} \quad (\text{C4})$$

which has all the polarization degrees of freedom necessary to form the various physical processes to be discussed next.

The contribution of the Hamiltonian in Eq. (4), H_{CA} is divided into two parts. First, the contribution of $H_{\text{CA}_1} = \hbar\eta \sum_i (\hat{a}^\dagger \hat{\sigma}_{02}^i + \hat{a} \hat{\sigma}_{20}^i)$ is given by,

$$\begin{aligned} \partial_t \mathcal{P}[n_{44}, n_{43}, n_{42}, \dots, n_{01}; k, p] | H_{\text{CA}_1} = & i\eta [(n_{24} + 1)\sqrt{k} \mathcal{P}[\dots, n_{24} + 1, \dots, n_{04} - 1, \dots; k - 1, p] \\ & + (n_{23} + 1)\sqrt{k} \mathcal{P}[\dots, n_{23} + 1, \dots, n_{03} - 1, \dots; k - 1, p] \\ & + (n_{22} + 1)\sqrt{k} \mathcal{P}[\dots, n_{22} + 1, \dots, n_{02} - 1, \dots; k - 1, p] \\ & + (n_{21} + 1)\sqrt{k} \mathcal{P}[\dots, n_{21} + 1, \dots, n_{01} - 1, \dots; k - 1, p] \\ & + (n_{20} + 1)\sqrt{k} \mathcal{P}[\dots, n_{20} + 1; k - 1, p] \\ & + (n_{04} + 1)\sqrt{k+1} \mathcal{P}[\dots, n_{04} + 1, \dots, n_{24} - 1; k + 1, p] \\ & + (n_{03} + 1)\sqrt{k+1} \mathcal{P}[\dots, n_{03} + 1, \dots, n_{23} - 1; k + 1, p] \\ & + (n_{02} + 1)\sqrt{k+1} \mathcal{P}[\dots, n_{02} + 1, \dots, n_{22} - 1; k + 1, p] \end{aligned}$$

$$\begin{aligned}
 &+ (n_{01} + 1)\sqrt{k + 1} \mathcal{P}[\dots n_{01} + 1 \dots n_{21} - 1; k + 1, p] \\
 &+ (n_{01} + 1)\sqrt{k + 1} \mathcal{P}[\dots n_{01} + 1 \dots n_{21} - 1; k + 1, p] \\
 &+ (n_{01} + 1)\sqrt{k + 1} \mathcal{P}[\dots n_{01} + 1 \dots n_{21} - 1; k + 1, p] \\
 &+ (n_{00} + 1)\sqrt{k + 1} \mathcal{P}[\dots n_{20} - 1 \dots; k + 1, p] \\
 &- (n_{40} + 1)\sqrt{p} \mathcal{P}[\dots n_{40} + 1 \dots n_{42} - 1 \dots; k, p - 1] \\
 &- (n_{30} + 1)\sqrt{p} \mathcal{P}[\dots n_{30} + 1 \dots n_{32} - 1 \dots; k, p - 1] \\
 &- (n_{20} + 1)\sqrt{p} \mathcal{P}[\dots n_{20} + 1 \dots n_{22} - 1 \dots; k, p - 1] \\
 &- (n_{10} + 1)\sqrt{p} \mathcal{P}[\dots n_{10} + 1 \dots n_{12} - 1 \dots; k, p - 1] \\
 &- (n_{00} + 1)\sqrt{p} \mathcal{P}[\dots n_{02} - 1; k, p - 1] \\
 &- (n_{42} + 1)\sqrt{p + 1} \mathcal{P}[\dots n_{42} + 1 \dots n_{40} - 1 \dots; k, p + 1] \\
 &- (n_{32} + 1)\sqrt{p + 1} \mathcal{P}[\dots n_{32} + 1 \dots n_{30} - 1 \dots; k, p + 1] \\
 &- (n_{22} + 1)\sqrt{p + 1} \mathcal{P}[\dots n_{22} + 1 \dots n_{20} - 1 \dots; k, p + 1] \\
 &- (n_{12} + 1)\sqrt{p + 1} \mathcal{P}[\dots n_{12} - 1 \dots n_{10} - 1 \dots; k, p + 1] \\
 &- (n_{02} + 1)\sqrt{p + 1} \mathcal{P}[\dots n_{02} + 1; k, p + 1]], \tag{C5}
 \end{aligned}$$

and second, the contribution of the Hamiltonian $H_{CA_2} = \hbar\eta \sum_i (\hat{a}^\dagger \hat{\sigma}_{13}^i + \hat{a} \hat{\sigma}_{31}^i)$ is given by

$$\begin{aligned}
 \partial_t \mathcal{P}[n_{44}, n_{43}, n_{42}, \dots n_{01}; k, p] |H_{CA_2} = & i\eta[(n_{14} + 1)\sqrt{k} \mathcal{P}[\dots n_{14} + 1 \dots n_{34} - 1 \dots; k - 1, p] \\
 & + (n_{13} + 1)\sqrt{k} \mathcal{P}[\dots n_{13} + 1 \dots n_{33} - 1 \dots; k - 1, p] \\
 & + (n_{12} + 1)\sqrt{k} \mathcal{P}[\dots n_{12} + 1 \dots n_{32} - 1 \dots; k - 1, p] \\
 & + (n_{11} + 1)\sqrt{k} \mathcal{P}[\dots n_{11} + 1 \dots n_{31} - 1 \dots; k - 1, p] \\
 & + (n_{10} + 1)\sqrt{k} \mathcal{P}[\dots n_{10} + 1 \dots n_{30} - 1 \dots; k - 1, p] \\
 & + (n_{34} + 1)\sqrt{k + 1} \mathcal{P}[\dots n_{34} + 1 \dots n_{14} - 1 \dots; k + 1, p] \\
 & + (n_{33} + 1)\sqrt{k + 1} \mathcal{P}[\dots n_{33} + 1 \dots n_{13} - 1 \dots; k + 1, p] \\
 & + (n_{32} + 1)\sqrt{k + 1} \mathcal{P}[\dots n_{32} + 1 \dots n_{12} - 1 \dots; k + 1, p] \\
 & + (n_{31} + 1)\sqrt{k + 1} \mathcal{P}[\dots n_{31} + 1 \dots n_{11} - 1 \dots; k + 1, p] \\
 & + (n_{30} + 1)\sqrt{k + 1} \mathcal{P}[\dots n_{30} + 1 \dots n_{10} - 1 \dots; k + 1, p] \\
 & - (n_{43} + 1)\sqrt{p} \mathcal{P}[\dots n_{43} + 1 \dots n_{41} - 1 \dots; k, p - 1] \\
 & - (n_{33} + 1)\sqrt{p} \mathcal{P}[\dots n_{33} + 1 \dots n_{31} - 1 \dots; k, p - 1] \\
 & - (n_{23} + 1)\sqrt{p} \mathcal{P}[\dots n_{23} + 1 \dots n_{21} - 1 \dots; k, p - 1] \\
 & - (n_{13} + 1)\sqrt{p} \mathcal{P}[\dots n_{13} + 1 \dots n_{11} - 1 \dots; k, p - 1] \\
 & - (n_{03} + 1)\sqrt{p} \mathcal{P}[\dots n_{03} + 1 \dots n_{01} - 1 \dots; k, p - 1] \\
 & - (n_{41} + 1)\sqrt{p + 1} \mathcal{P}[\dots n_{41} + 1 \dots n_{43} - 1 \dots; k, p + 1] \\
 & - (n_{31} + 1)\sqrt{p + 1} \mathcal{P}[\dots n_{31} + 1 \dots n_{33} - 1 \dots; k, p + 1] \\
 & - (n_{21} + 1)\sqrt{p + 1} \mathcal{P}[\dots n_{21} + 1 \dots n_{23} - 1 \dots; k, p + 1]
 \end{aligned}$$

$$\begin{aligned}
& - (n_{11} + 1)\sqrt{p+1} \mathcal{P}[\dots n_{11} - 1 \dots n_{13} - 1 \dots; k, p+1] \\
& - (n_{01} + 1)\sqrt{p+1} \mathcal{P}[\dots n_{01} + 1 \dots n_{03} - 1 \dots; k, p+1]. \tag{C6}
\end{aligned}$$

The construction of these physical operators depends on whether the operators act from the right or left of the density matrix. Further technical details of defining these mathematical equations are provided in Refs. [50,52].

Next we introduce the coherent pumping Hamiltonian H_{LA} , which is divided into three parts, $H_{LA} = H_{LA_1} + H_{LA_2} + H_{LA_3}$. First, $H_{LA_1} = \hbar\Omega_1 \sum_i (\hat{\sigma}_{21}^i + \hat{\sigma}_{12}^i)$, which is given by

$$\begin{aligned}
\partial_t \mathcal{P}[n_{44}, n_{43}, n_{42}, \dots n_{01}; k, p] | H_{LA_1} = & i\Omega_1 [(n_{14} + 1)\sqrt{k} \mathcal{P}[\dots n_{14} + 1 \dots n_{24} - 1 \dots; k-1, p] \\
& + (n_{13} + 1)\sqrt{k} \mathcal{P}[\dots n_{13} + 1 \dots n_{23} - 1 \dots; k-1, p] \\
& + (n_{12} + 1)\sqrt{k} \mathcal{P}[\dots n_{12} + 1 \dots n_{22} - 1 \dots; k-1, p] \\
& + (n_{11} + 1)\sqrt{k} \mathcal{P}[\dots n_{11} + 1 \dots n_{21} - 1 \dots; k-1, p] \\
& + (n_{10} + 1)\sqrt{k} \mathcal{P}[\dots n_{10} + 1 \dots n_{20} - 1 \dots; k-1, p] \\
& + (n_{24} + 1)\sqrt{k+1} \mathcal{P}[\dots n_{24} + 1 \dots n_{14} - 1 \dots; k+1, p] \\
& + (n_{23} + 1)\sqrt{k+1} \mathcal{P}[\dots n_{23} + 1 \dots n_{13} - 1 \dots; k+1, p] \\
& + (n_{22} + 1)\sqrt{k+1} \mathcal{P}[\dots n_{22} + 1 \dots n_{12} - 1 \dots; k+1, p] \\
& + (n_{21} + 1)\sqrt{k+1} \mathcal{P}[\dots n_{21} + 1 \dots n_{11} - 1 \dots; k+1, p] \\
& + (n_{20} + 1)\sqrt{k+1} \mathcal{P}[\dots n_{20} + 1 \dots n_{10} - 1 \dots; k+1, p] \\
& - (n_{41} + 1)\sqrt{p} \mathcal{P}[\dots n_{41} + 1 \dots n_{42} - 1 \dots; k, p-1] \\
& - (n_{31} + 1)\sqrt{p} \mathcal{P}[\dots n_{31} + 1 \dots n_{32} - 1 \dots; k, p-1] \\
& - (n_{21} + 1)\sqrt{p} \mathcal{P}[\dots n_{21} + 1 \dots n_{22} - 1 \dots; k, p-1] \\
& - (n_{11} + 1)\sqrt{p} \mathcal{P}[\dots n_{11} + 1 \dots n_{12} - 1 \dots; k, p-1] \\
& - (n_{01} + 1)\sqrt{p} \mathcal{P}[\dots n_{01} + 1 \dots n_{02} - 1 \dots; k, p-1] \\
& - (n_{42} + 1)\sqrt{p+1} \mathcal{P}[\dots n_{42} + 1 \dots n_{41} - 1 \dots; k, p+1] \\
& - (n_{32} + 1)\sqrt{p+1} \mathcal{P}[\dots n_{32} + 1 \dots n_{31} - 1 \dots; k, p+1] \\
& - (n_{22} + 1)\sqrt{p+1} \mathcal{P}[\dots n_{22} + 1 \dots n_{21} - 1 \dots; k, p+1] \\
& - (n_{12} + 1)\sqrt{p+1} \mathcal{P}[\dots n_{12} - 1 \dots n_{11} - 1 \dots; k, p+1] \\
& - (n_{02} + 1)\sqrt{p+1} \mathcal{P}[\dots n_{02} + 1 \dots n_{01} - 1 \dots; k, p+1]. \tag{C7}
\end{aligned}$$

Second, the contribution of the Hamiltonian $H_{LA_2} = \hbar\Omega_2 \sum_i (\hat{\sigma}_{30}^i + \hat{\sigma}_{03}^i)$ is given by

$$\begin{aligned}
\partial_t \mathcal{P}[n_{44}, n_{43}, n_{42}, \dots n_{01}; k, p] | H_{LA_2} = & i\Omega_2 [(n_{34} + 1)\sqrt{k} \mathcal{P}[\dots n_{34} + 1 \dots n_{04} - 1 \dots; k-1, p] \\
& + (n_{33} + 1)\sqrt{k} \mathcal{P}[\dots n_{33} + 1 \dots n_{03} - 1 \dots; k-1, p] \\
& + (n_{32} + 1)\sqrt{k} \mathcal{P}[\dots n_{32} + 1 \dots n_{02} - 1 \dots; k-1, p] \\
& + (n_{31} + 1)\sqrt{k} \mathcal{P}[\dots n_{31} + 1 \dots n_{01} - 1 \dots; k-1, p] \\
& + (n_{30} + 1)\sqrt{k} \mathcal{P}[\dots n_{30} + 1 \dots; k-1, p] \\
& + (n_{04} + 1)\sqrt{k+1} \mathcal{P}[\dots n_{04} + 1 \dots n_{34} - 1 \dots; k+1, p] \\
& + (n_{03} + 1)\sqrt{k+1} \mathcal{P}[\dots n_{03} + 1 \dots n_{33} - 1 \dots; k+1, p]
\end{aligned}$$

$$\begin{aligned}
& + (n_{02} + 1)\sqrt{k+1} \mathcal{P}[\dots n_{02} + 1 \dots n_{32} - 1 \dots; k+1, p] \\
& + (n_{01} + 1)\sqrt{k+1} \mathcal{P}[\dots n_{01} + 1 \dots n_{31} - 1 \dots; k+1, p] \\
& + (n_{00} + 1)\sqrt{k+1} \mathcal{P}[\dots n_{30} - 1 \dots; k+1, p] \\
& - (n_{40} + 1)\sqrt{p} \mathcal{P}[\dots n_{40} + 1 \dots n_{43} - 1 \dots; k, p-1] \\
& - (n_{30} + 1)\sqrt{p} \mathcal{P}[\dots n_{30} + 1 \dots n_{33} - 1 \dots; k, p-1] \\
& - (n_{20} + 1)\sqrt{p} \mathcal{P}[\dots n_{20} + 1 \dots n_{23} - 1 \dots; k, p-1] \\
& - (n_{10} + 1)\sqrt{p} \mathcal{P}[\dots n_{10} + 1 \dots n_{13} - 1 \dots; k, p-1] \\
& - (n_{00} + 1)\sqrt{p} \mathcal{P}[\dots n_{03} - 1 \dots; k, p-1] \\
& - (n_{43} + 1)\sqrt{p+1} \mathcal{P}[\dots n_{43} + 1 \dots n_{40} - 1 \dots; k, p+1] \\
& - (n_{33} + 1)\sqrt{p+1} \mathcal{P}[\dots n_{33} + 1 \dots n_{30} - 1 \dots; k, p+1] \\
& - (n_{23} + 1)\sqrt{p+1} \mathcal{P}[\dots n_{23} + 1 \dots n_{20} - 1 \dots; k, p+1] \\
& - (n_{13} + 1)\sqrt{p+1} \mathcal{P}[\dots n_{13} - 1 \dots n_{10} - 1 \dots; k, p+1] \\
& - (n_{03} + 1)\sqrt{p+1} \mathcal{P}[\dots n_{03} + 1 \dots; k, p+1].
\end{aligned} \tag{C8}$$

Third, the contribution of the Hamiltonian $H_{LA_3} = \hbar\Omega_c \sum_i (\hat{\sigma}_{42}^i + \hat{\sigma}_{24}^i)$ is given by

$$\begin{aligned}
\partial_t \mathcal{P}[n_{44}, n_{43}, n_{42}, \dots n_{01}; k, p] |H_{LA_3} = & i\Omega_c [(n_{44} + 1)\sqrt{k} \mathcal{P}[\dots n_{44} + 1 \dots n_{24} - 1 \dots; k-1, p] \\
& + (n_{43} + 1)\sqrt{k} \mathcal{P}[\dots n_{43} + 1 \dots n_{23} - 1 \dots; k-1, p] \\
& + (n_{42} + 1)\sqrt{k} \mathcal{P}[\dots n_{42} + 1 \dots n_{22} - 1 \dots; k-1, p] \\
& + (n_{41} + 1)\sqrt{k} \mathcal{P}[\dots n_{41} + 1 \dots n_{21} - 1 \dots; k-1, p] \\
& + (n_{40} + 1)\sqrt{k} \mathcal{P}[\dots n_{40} + 1 \dots n_{20} - 1 \dots; k-1, p] \\
& + (n_{24} + 1)\sqrt{k+1} \mathcal{P}[\dots n_{24} + 1 \dots n_{44} - 1 \dots; k+1, p] \\
& + (n_{23} + 1)\sqrt{k+1} \mathcal{P}[\dots n_{23} + 1 \dots n_{43} - 1 \dots; k+1, p] \\
& + (n_{22} + 1)\sqrt{k+1} \mathcal{P}[\dots n_{22} + 1 \dots n_{42} - 1 \dots; k+1, p] \\
& + (n_{21} + 1)\sqrt{k+1} \mathcal{P}[\dots n_{21} + 1 \dots n_{41} - 1 \dots; k+1, p] \\
& + (n_{20} + 1)\sqrt{k+1} \mathcal{P}[\dots n_{20} + 1 \dots n_{40} - 1 \dots; k+1, p] \\
& - (n_{42} + 1)\sqrt{p} \mathcal{P}[\dots n_{42} + 1 \dots n_{44} - 1 \dots; k, p-1] \\
& - (n_{32} + 1)\sqrt{p} \mathcal{P}[\dots n_{32} + 1 \dots n_{34} - 1 \dots; k, p-1] \\
& - (n_{22} + 1)\sqrt{p} \mathcal{P}[\dots n_{22} + 1 \dots n_{24} - 1 \dots; k, p-1] \\
& - (n_{12} + 1)\sqrt{p} \mathcal{P}[\dots n_{12} + 1 \dots n_{14} - 1 \dots; k, p-1] \\
& - (n_{02} + 1)\sqrt{p} \mathcal{P}[\dots n_{02} + 1 \dots n_{04} - 1 \dots; k, p-1] \\
& - (n_{44} + 1)\sqrt{p+1} \mathcal{P}[\dots n_{44} + 1 \dots n_{42} - 1 \dots; k, p+1] \\
& - (n_{34} + 1)\sqrt{p+1} \mathcal{P}[\dots n_{34} + 1 \dots n_{32} - 1 \dots; k, p+1] \\
& - (n_{24} + 1)\sqrt{p+1} \mathcal{P}[\dots n_{24} + 1 \dots n_{22} - 1 \dots; k, p+1] \\
& - (n_{14} + 1)\sqrt{p+1} \mathcal{P}[\dots n_{14} + 1 \dots n_{12} - 1 \dots; k, p+1] \\
& - (n_{04} + 1)\sqrt{p+1} \mathcal{P}[\dots n_{04} + 1 \dots n_{02} - 1 \dots; k, p+1].
\end{aligned} \tag{C9}$$

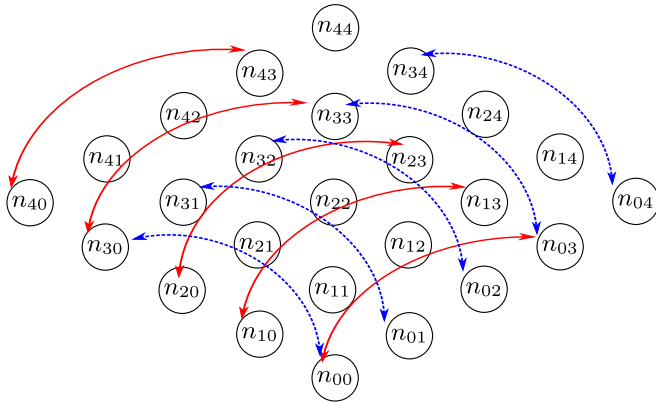


FIG. 10. Contribution of optical pumping of the system Ω_2 ; densities are exchanged between n_{33} and n_{00} (red solid lines and blue dashed lines) via the build up of quantum coherence. This graph corresponds to the Lindblad equation given in Eq. (C8).

The next step is to draw the sketch for the required Liouville operators for each specific finding. The sketches are shown in Figs. 8–11. The coupling processes are represented by an arrow connecting two distinguished symmetric states. For the noninteracting Hamiltonian part, which is included in the calculations, we use nonconnecting arrows. The pictorial representation of the nonconnecting arrows are not shown in the figures (Figs. 8–11) but they are included in the formulation and the numerical simulation of our work. We use the L, R algebra to determine the elementary Liouville operators in implementing the code. A Liouville space operator is defined

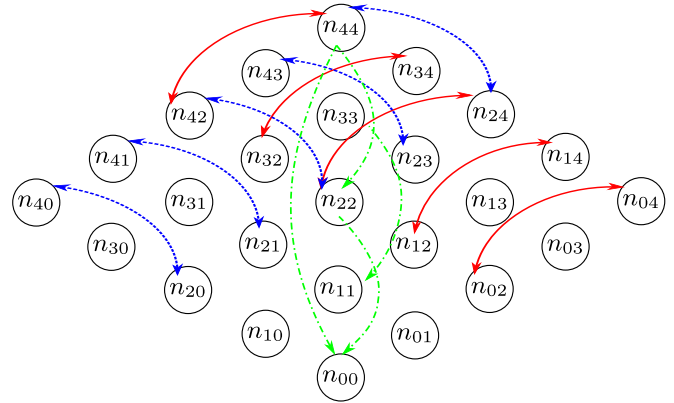


FIG. 11. Contribution of optical pumping of the system Ω_c ; densities are exchanged between n_{44} and n_{33} (red solid lines and blue dashed lines) via the build up of quantum coherence. This graph corresponds to the Lindblad equation given in Eq. (C9). Action of the Lindblad dissipators: green (dash-dot) arrows describe spontaneous emission.

by discerning whether it acts on the left (L) or right (R) side of the density matrix [50], i.e., $A\hat{\rho} = A^L\hat{\rho}$ and $\hat{\rho}A = A^R\hat{\rho}$. For example, the definition of a collective spontaneous emission Liouvillian from level a to level b is

$$\begin{aligned} \mathcal{L}(\hat{\rho}) &= \frac{\gamma}{2} (\hat{J}_{ba}\hat{\rho}\hat{J}_{ab} - \hat{J}_{ab}\hat{J}_{ba}\hat{\rho} - \hat{\rho}\hat{J}_{ab}\hat{J}_{ba}) \\ &= \frac{\gamma}{2} (\hat{J}_{ba}^L \cdot \hat{J}_{ab}^R - \hat{J}_{ab}^L \cdot \hat{J}_{ba}^L - \hat{J}_{ba}^R \cdot \hat{J}_{ab}^R) \hat{\rho}. \end{aligned} \quad (\text{C10})$$

In a similar way we can build the rest of the system.

-
- [1] D. Craig and T. Thirunamachandran, *Molecular Quantum Electrodynamics* (Dover, New York, 1998).
- [2] M. Premaratne and G. P. Agrawal, *Light Propagation in Gain Media: Optical Amplifiers* (Cambridge University Press, Cambridge, 2011).
- [3] R. T. Wijesekara, S. D. Gunapala, and M. Premaratne, *Phys. Rev. B* **104**, 045405 (2021).
- [4] T. Perera, S. D. Gunapala, M. I. Stockman, and M. Premaratne, *J. Phys. Chem. C* **124**, 27694 (2020).
- [5] S. Pathirana, S. D. Gunapala, and M. Premaratne, *J. Phys.: Condens. Matter* **33**, 245301 (2021).
- [6] S. Haroche and J.-M. Raimond, *Exploring the Quantum: Atoms, Cavities, and Photons* (Oxford University Press, Oxford, 2006).
- [7] M. Premaratne and G. P. Agrawal, *Theoretical Foundations of Nanoscale Quantum Devices* (Cambridge University Press, Cambridge, 2020).
- [8] Y. Kaluzny, P. Goy, M. Gross, J. M. Raimond, and S. Haroche, *Phys. Rev. Lett.* **51**, 1175 (1983).
- [9] J.-M. Raimond, M. Brune, and S. Haroche, *Rev. Mod. Phys.* **73**, 565 (2001).
- [10] F. Brennecke, T. Donner, S. Ritter, T. Bourdel, M. Köhl, and T. Esslinger, *Nature (London)* **450**, 268 (2007).
- [11] Q. Zhang, M. Lou, X. Li, J. L. Reno, W. Pan, J. D. Watson, M. J. Manfra, and J. Kono, *Nat. Phys.* **12**, 1005 (2016).
- [12] J. P. Reithmaier, G. Sęk, A. Löffler, C. Hofmann, S. Kuhn, S. Reitzenstein, L. Keldysh, V. Kulakovskii, T. Reinecke, and A. Forchel, *Nature (London)* **432**, 197 (2004).
- [13] A. Wallraff, D. I. Schuster, A. Blais, L. Frunzio, R.-S. Huang, J. Majer, S. Kumar, S. M. Girvin, and R. J. Schoelkopf, *Nature (London)* **431**, 162 (2004).
- [14] M. Mazzeo, A. Genco, S. Gambino, D. Ballarini, F. Mangione, O. Di Stefano, S. Patanè, S. Savasta, D. Sanvitto, and G. Gigli, *Appl. Phys. Lett.* **104**, 233303 (2014).
- [15] C. Weisbuch, M. Nishioka, A. Ishikawa, and Y. Arakawa, *Phys. Rev. Lett.* **69**, 3314 (1992).
- [16] J. McKeever, A. Boca, A. D. Boozer, J. R. Buck, and H. J. Kimble, *Nature (London)* **425**, 268 (2003).
- [17] T. Aoki, B. Dayan, E. Wilcut, W. P. Bowen, A. S. Parkins, T. Kippenberg, K. Vahala, and H. Kimble, *Nature (London)* **443**, 671 (2006).
- [18] S. M. Spillane, T. J. Kippenberg, K. J. Vahala, K. W. Goh, E. Wilcut, and H. J. Kimble, *Phys. Rev. A* **71**, 013817 (2005).
- [19] F. Dimer, B. Estienne, A. S. Parkins, and H. J. Carmichael, *Phys. Rev. A* **75**, 013804 (2007).
- [20] F. D. De Oliveira, Ph.D. thesis, University of Auckland, 2008.
- [21] Z. Zhang, C. H. Lee, R. Kumar, K. J. Arnold, S. J. Masson, A. L. Grimsmo, A. S. Parkins, and M. D. Barrett, *Phys. Rev. A* **97**, 043858 (2018).

- [22] K. Baumann, C. Guerlin, F. Brennecke, and T. Esslinger, *Nature (London)* **464**, 1301 (2010).
- [23] A. L. Grimsmo and S. Parkins, *Phys. Rev. A* **87**, 033814 (2013).
- [24] A. Grimsmo and A. Parkins, *J. Phys. B: At. Mol. Opt. Phys.* **46**, 224012 (2013).
- [25] A. Devi, S. D. Gunapala, M. I. Stockman, and M. Premaratne, *Phys. Rev. A* **102**, 013701 (2020).
- [26] Z. Zhiqiang, C. H. Lee, R. Kumar, K. J. Arnold, S. J. Masson, A. S. Parkins, and M. D. Barrett, *Optica* **4**, 424 (2017).
- [27] K. E. Dorfman, P. K. Jha, D. V. Voronine, P. Genevet, F. Capasso, and M. O. Scully, *Phys. Rev. Lett.* **111**, 043601 (2013).
- [28] E. P. Ostby, *Photonic Whispering-Gallery Resonators in New Environments* (California Institute of Technology, Pasadena, 2009).
- [29] M. P. Baden, K. J. Arnold, A. L. Grimsmo, S. Parkins, and M. D. Barrett, *Phys. Rev. Lett.* **113**, 020408 (2014).
- [30] K. J. Arnold, M. P. Baden, and M. D. Barrett, *Phys. Rev. Lett.* **109**, 153002 (2012).
- [31] K. C. Stitely, S. J. Masson, A. Giraldo, B. Krauskopf, and S. Parkins, *Phys. Rev. A* **102**, 063702 (2020).
- [32] T. Wilk, H. P. Specht, S. C. Webster, G. Rempe, and A. Kuhn, *J. Mod. Opt.* **54**, 1569 (2007).
- [33] D. A. Steck, Rubidium 87 D line data, 2001.
- [34] L. Kumarapperuma, M. Premaratne, P. K. Jha, M. I. Stockman, and G. P. Agrawal, *Appl. Phys. Lett.* **112**, 201108 (2018).
- [35] M. Premaratne and M. I. Stockman, *Adv. Opt. Photon.* **9**, 79 (2017).
- [36] N. Shammah, S. Ahmed, N. Lambert, S. De Liberato, and F. Nori, *Phys. Rev. A* **98**, 063815 (2018).
- [37] B. Zhu, J. Cooper, J. Ye, and A. M. Rey, *Phys. Rev. A* **94**, 023612 (2016).
- [38] P. Meystre and M. Sargent, *Elements of Quantum Optics* (Springer Science & Business Media, Berlin, 2007).
- [39] R. T. Wijesekara, S. D. Gunapala, M. I. Stockman, and M. Premaratne, *Phys. Rev. B* **101**, 245402 (2020).
- [40] T. Warnakula, S. D. Gunapala, M. I. Stockman, and M. Premaratne, *Phys. Rev. B* **100**, 085439 (2019).
- [41] N. De Silva, T. Warnakula, S. D. Gunapala, M. I. Stockman, and M. Premaratne, *J. Phys.: Condens. Matter* **33**, 145304 (2021).
- [42] H. Breuer and F. Petruccione, *The Theory of Open Quantum Systems* (Oxford University Press, Oxford, 2002).
- [43] M. J. Bhaseen, J. Mayoh, B. D. Simons, and J. Keeling, *Phys. Rev. A* **85**, 013817 (2012).
- [44] D. Meiser, J. Ye, D. R. Carlson, and M. J. Holland, *Phys. Rev. Lett.* **102**, 163601 (2009).
- [45] J. G. Bohnet, Z. Chen, J. M. Weiner, K. C. Cox, and J. K. Thompson, *Phys. Rev. Lett.* **109**, 253602 (2012).
- [46] H. Hapuarachchi, M. Premaratne, Q. Bao, W. Cheng, S. D. Gunapala, and G. P. Agrawal, *Phys. Rev. B* **95**, 245419 (2017).
- [47] S. Mallawaarachchi, S. D. Gunapala, M. I. Stockman, and M. Premaratne, *Phys. Rev. B* **97**, 125406 (2018).
- [48] M. O. Scully and M. S. Zubairy, *Quantum Optics* (American Association of Physics Teachers, 1999).
- [49] P. Jha, A. Svidzinsky, and M. Scully, *Laser Phys. Lett.* **9**, 368 (2012).
- [50] M. Gegg and M. Richter, *Sci. Rep.* **7**, 16304 (2017).
- [51] J. R. Johansson, P. D. Nation, and F. Nori, *Comput. Phys. Commun.* **184**, 1234 (2013).
- [52] M. Gegg, Identical emitters, collective effects and dissipation in quantum optics, Technical University of Berlin (2017).
- [53] P. Kirton and J. Keeling, *New J. Phys.* **20**, 015009 (2018).
- [54] S. Kéna-Cohen, S. A. Maier, and D. D. Bradley, *Adv. Opt. Mater.* **1**, 827 (2013).
- [55] J. Flick, M. Ruggenthaler, H. Appel, and A. Rubio, *Proc. Natl. Acad. Sci. USA* **114**, 3026 (2017).
- [56] B. Liu, W. Zhu, S. D. Gunapala, M. I. Stockman, and M. Premaratne, *ACS Nano* **11**, 12573 (2017).
- [57] C. Jayasekara, M. Premaratne, S. D. Gunapala, and M. I. Stockman, *J. Appl. Phys.* **119**, 133101 (2016).
- [58] W. Zhu, I. D. Rukhlenko, and M. Premaratne, *J. Opt. Soc. Am. B* **29**, 2659 (2012).
- [59] A. F. Kockum, A. Miranowicz, S. De Liberato, S. Savasta, and F. Nori, *Nat. Rev. Phys.* **1**, 19 (2019).
- [60] P. Kirton and J. Keeling, *Phys. Rev. Lett.* **118**, 123602 (2017).